

# **Layer 2/3 Pyramidal Neurons: Characterization of Anatomy and Synaptic Plasticity**

Rina Veler

**THESIS SUBMITTED IN PARTIAL FULFILLMENT OF THE  
REQUIREMENTS FOR THE MASTER'S DEGREE**

University of Haifa  
Faculty of Natural Sciences  
Sagol Department of Neurobiology

February, 2019

# **Layer 2/3 Pyramidal Neurons: Characterization of Anatomy and Synaptic Plasticity**

By: Rina Veler

Supervised by: Dr. Lior Cohen

## **THESIS SUBMITTED IN PARTIAL FULFILLMENT OF THE REQUIREMENTS FOR THE MASTER'S DEGREE**

University of Haifa  
Faculty of Natural Sciences  
Sagol Department of Neurobiology

February, 2019

Approved by: \_\_\_\_\_ Date: \_\_\_\_\_  
(Supervisor)

Approved by: \_\_\_\_\_ Date: \_\_\_\_\_  
(Chairperson of Master's studies Committee)

## Gratitude

First of all, I want to dedicate my work to my dear father Haim Kleinman, blessed memory, who always encouraged and supported me to learn and to do my best with simplicity and humility. All of my achievements are thanks to him and I'm sure it makes him happy.

I owe a huge gratitude to my supervisor, the one and only, Dr. Lior Cohen, for all the professional guidance, the endless support, personal attention, encouragement, patience and the list goes on. I had the pleasure and privilege of being Dr. Lior Cohen's first master student and I am convinced that many others would enjoy being under his guidance.

Special thanks to Mr. Elad Mazaki, who conceived the idea of creating geometric rules to test the anatomical 'blue print' of L2/3 PyrNs. I owe him thanks for dedicating his time to give me a private guidance on using Python, patiently answering my questions and solving my problems. Mr. Elad Mazaki added a particularly significant and positive element to my work.

My heartfelt thanks to my beloved family (especially my mother Rachel, my husband Ariel and Noga, our sweet daughter) for all the help, motivation, support and interest during the last three years which enabled me to advance in the research and successfully complete it. This accomplishment would not have been possible without them.

Finally, my thanks go to all the people who have supported me, directly or indirectly, so I could complete the research.

## Table of Contents

Abstract .....	IV
List of Tables.....	V
List of Figures .....	VI
List of abbreviations.....	VII
1. Introduction .....	1
2. Research Goals.....	5
3. Hypothesis.....	6
4. Materials and Methods .....	7
4.1. Surgical Procedures.....	7
4.2. Electrophysiology and Electroporation .....	7
4.3. Imaging .....	8
4.4. Analysis of <i>in vivo</i> structural data.....	8
5. Results .....	10
5.1. Data processing: .....	10
5.2. Parameters extraction and validation: .....	13
5.3. Parameter Analysis:.....	19
5.4. Preparation of other datasets: .....	25
5.5. Meta data analysis: .....	31
6. Discussion .....	36
6.1. Structural plasticity of PyrNs .....	36
6.2. Mouse L2/3 PyrNs anatomical blueprint.....	37
6.3. L2/3 PyrNs anatomical blueprint conservation .....	39
References .....	41
Appendix 1: Layer 2/3 PyrNs reconstruction.....	45

# **Layer 2/3 Pyramidal Neurons: Characterization of Anatomy and Synaptic Plasticity**

Rina Veler

## **Abstract**

Over the last 150 years, much has been written about the most widespread cells in the cerebral cortex, the pyramidal neurons (PyrNs). This vast neuronal population has been considered to be a homogeneous population with a very unique morphology, when compared to other neuronal populations, such as interneurons, which are small in number but exhibit large diversity. However, a variety of PyrNs can be found in different brain regions and within the layered neocortex. This variety is characterized by different features, including neuroanatomy, location, projection targets, plasticity etc. Each cortical PyrN has different function depending on its particular features. Thus, detailed description of PyrNs neuroanatomy and synaptic plasticity might lead to a better understanding of cortical circuits.

Layer 2/3 is one of the six layers of the neocortex, which is considered to be a key integration point of various inputs from broad regions in the brain. However, the information regarding the PyrNs constituting this layer is limited. In this research, we performed a multi-parameter analysis of L2/3 PyrNs neuroanatomy and synaptic plasticity rates based on time lapse *in vivo* imaging, in order to construct a set of anatomical and connectivity rules describing this circuit. We further tested PyrNs in other mammals and found that they also obey to this set of rules, implying those rules to be universal. The analysis described here is essential for understanding computational processes, sensory processing, function and connectivity in this fundamental layer of the neocortex.

## **List of Tables**

Table 1: Synaptic Plasticity Correlations. ....	19
---	----

## List of Figures

Figure 1: Input-output relationships of cortex.....	2
Figure 2: Data pre-processing flowchart.....	9
Figure 3: Synaptic plasticity pre-processing.....	12
Figure 4: Neuroanatomy pre-processing.....	13
Figure 5: Synaptic structure neurite types comparing.....	16
Figure 6: Two time points reconstruction comparisons.....	18
Figure 7: Correlations between synaptic plasticity and depth.....	19
Figure 8: Parameters distribution.....	20
Figure 9: Different structures of L2/3 PyrNs.....	21
Figure 10: Correlations color maps.....	23
Figure 11: Linear regression correlations between parameters.....	24
Figure 12: Our dataset parameters distribution.....	27
Figure 13: Mouse L2/3 parameters distribution.....	28
Figure 14: Rat L2/3 parameters distribution.....	29
Figure 15: Human L2/3 parameters distribution.....	30
Figure 16: Rat L5 parameters distribution.....	31
Figure 17: Rat INs parameters distribution.....	32
Figure 18: Comparison of correlations color maps.....	34
Figure 19: MSE's significance of different datasets.....	35

## **List of abbreviations**

AC	Auditory Cortex
AD	Apical Dendrite
AX	Axon
BD	Basal Dendrite
FDR	False Discovery Rate
FFT	Fast Fourier Transform
INs	Inhibitory Neurons
L1	Layer 1
L2/3	Layer 2/3
L4	Layer 4
L5	Layer 5
L6	Layer 6
LUT	LookUp Table
PyrNs	Pyramidal Neurons
SSP	Structural Synaptic Plasticity

## **1. Introduction**

Pyramidal neurons (PyrNs) are abundant in the neocortex of all mammals. PyrNs were first discovered by Santiago Ramón y Cajal (Elston, 2003). Those neurons are found in forebrain structures such as the cerebral cortex, hippocampus, and amygdala, but not in the olfactory bulbs, striatum, midbrain, hindbrain, or spinal cord. Since they are the most abundant type of glutamatergic excitatory cells in mammalian cortical structures, it is reasonable that they play important roles in advanced cognitive functions (Ramón y Cajal, 1995). The structure of PyrNs is quite variable, both between regions (e.g. hippocampus vs neocortex) and within regions (e.g. L2 vs L5 of neocortex) (Spruston, 2008). Nevertheless, PyrNs have a stereotypical morphology, which one of the main structural features is the triangular shaped soma (Megías, Emri, Freund & Gulyás, 2001). Other key structural features are the single AX and separate basal and apical trees which descend from the base and the apex of the soma, respectively (Spruston, 2008). PyrNs represent the vast majority of neocortical cells (about 80–90%), the remaining being constituted by GABAergic, INs (Noback, 2005).

In the mammalian brain, the neocortex contains six layers arranged in parallel to the cortical surface, in which the most superficial is L1. Different layers of the cortex have different function in converging inputs from different thalamic nuclei, other cortical areas, and several neuromodulatory systems with respect to its afferent and efferent connections (Figure 1) (Rodney & Kevan, 2004). L1 is primarily a receiving area for nonspecific afferent fibers from the intralaminar, thalamus and brainstem monoaminergic neurons. Sensory inputs relayed by the thalamus mainly influence the “granular” L4, which in turn signals to the other layers. The deep infragranular L5 and L6 are the main source of cortical outputs to subcortical structures, and L2/3 contributes an important source of projections to other cortical areas. This layer, receives from, and sends information to, many other neocortical regions and is therefore positioned as a key point in the network for integrating information across inter and intra cortical areas (Petersen & Crochet, 2013).

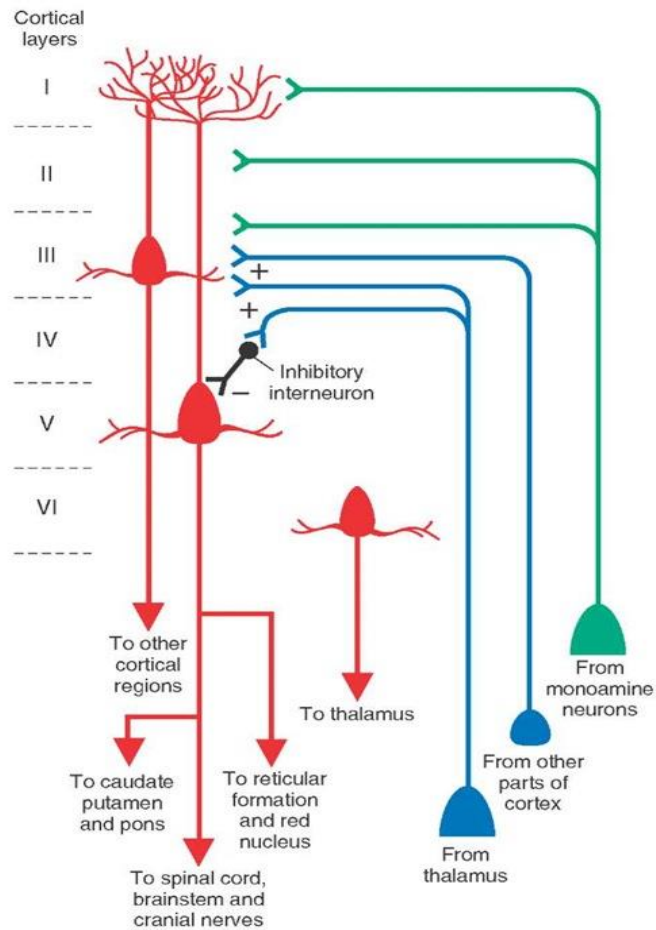


**Figure 1: Input-output relationships of the cortex. Schematic diagram depicts the intrinsic organization and input-output relationships of the cerebral cortex.**

Excitatory connections are indicated by (+), and inhibitory synapse is indicated by (-). Note that thalamocortical and intracortical projections terminate mainly in layer IV, and monoaminergic projections are distributed mainly to layers that are more superficial. Cortical afferents terminating in layer IV can either excite or inhibit pyramidal cells in layer V, which contribute significantly to the outputs of the cerebral cortex. The major outputs to the spinal cord, cranial nerve motor nuclei, other brainstem structures, thalamus, and neostriatum arise in layers V-VI, whereas projections to other regions of cortex either on the ipsilateral or contralateral side arise from layer III (adopted from <http://what-when-how.com/neuroscience/the-thalamus-and-cerebral-cortex-integrative-systems-part-1/>).

Cortical neurons may be characterized by a variety of features, such as their location, projection targets, dendritic and axonal morphology, electrophysiological properties, synaptic plasticity, and the identity of their neurotransmitters. Surprisingly, INs, though minor in number, are characterized by a great variety of anatomical features, electrophysiological properties, and connectivity patterns (Moore, Carlen, Knoblich & Cardin, 2010). Conversely, PyrNs are often conceived as a rather homogeneous population (Granato & De Giorgio, 2014). Indeed, prior to the advent of molecular markers, a PyrN's position within the six layered neocortex was the only available criteria to distinguish different subtypes. Recent

molecular, anatomical, and physiological methods have enhanced our ability to study PyrNs. Knowing how different aspects of neuronal phenotype are related is important for understanding neuronal function, connectivity and thus the function of the circuit. In particular, there is an inseparable link between the structure of a neuron and its function (Helbling et al., 2015; Spruston, 2008). Today we know that variability exists both across and within layers (Bannister, 2005). For example, in Ueta's research (Ueta, Otsuka, Morishima, Ushimaru, & Kawaguchi, 2014), they found some PyrNs subtypes in L5 in the motor cortex which characterized by their distinguished projection to other areas. Another example is the work of Steger et al. (Steger et al., 2013), which studied the "inverted" PyrNs in infragranular layers, whose AD turn to the white matter rather than pia surface.

Since the development of high-resolution optical imaging techniques, there is focused attention on the superficial layers of the mouse neocortex, which are readily accessible using current *in vivo* microscopy methods compared to infragranular layers, which are mainly accessible via *in vitro* electrophysiological methods. Searching the term "neuronal calcium imaging" at Pubmed website, produces approximately 5000 studies that investigate the population activity of between 100 to 1000 neurons by monitoring modifications in calcium concentrations. Sadakane et al. (Sadakane et al., 2015), for example, used two photon calcium imaging to investigate the neuronal populations in L1-L3 in adult non-human primates. They succeeded to (1) simultaneously record hundreds of neurons, (2) repeatedly image the same neuronal populations over weeks and months, and (3) reliably detect calcium transients in dendrites and axonal boutons. Two photon *in vivo* imaging is also suitable for monitoring L2/3 PyrNs anatomy as well as their synaptic structure over time (Holmaat et al., 2005; Trachtenberg et al., 2002; De Paola et al., 2006). The changes in pre-synaptic (boutons) and post-synaptic (spines) anatomical structures over time could provide new perspective to explore the relationship between neuron's anatomical structure and their SSP, i.e. rewiring within the circuit.

There is a dissension concerning the variability of PyrNs in the cortex, specifically in L2/3. Several studies have revealed a large diversity in cortical L2/3 PyrNs morphology (Hardingham, Gould, & Fox, 2011). They found that the "classical" PyrNs (with a prominent AD and limited horizontal dendritic spread) make up only a fraction of the L2/3 PyrNs in mouse barrel cortex. 50% of neurons had a main ADs skewed substantially away from the vertical, either in a medial or in a lateral direction and therefore had highly asymmetric arborizations. In addition, they found that the angle of the main AD to the columnar axis was not correlated with the distance of the soma from the pia. Moreover, Aerde and Feldmeyer

(Aerde & Feldmeyer, 2013), that studied the PyrNs subtypes in the medial prefrontal cortex in rats across all six layers, found a quite homogeneous population in L2 but four different subtypes in L3. L3 PyrNs mostly differ in their AD tuft and electrophysiological features. However, other studies have not found such differences (Mason & Larkman, 1990; Oberlaender et al., 2011).

The disagreement in this field might be due to the large variety of many different technics to discern between neurons subtypes. Despite the dispute between researches regarding the diversity of L2/3 PyrNs, neither of those researches investigated if there is fixed or differential relationship between independent structural features in the population of PyrNs. For example: Is there a relationship between the AX length of the cell and the number of its dendritic neurites, or its electrophysiological properties? Would knowing about one feature would enable us to predict other features i.e. are there any common rules for a PyrNs anatomical 'blueprint'? Those questions, and more, remained open.

Moreover, it is known that there are differences in the neocortex structures between species. According to Mohan at al. (Mohan et al., 2015) in the human temporal cortex, L2/3 was found to be particularly thick ( $949 \pm 179 \mu\text{m}$ ), compared to other investigated species like rats ( $\sim 350 \mu\text{m}$ ) (Gabbott, Warner, Jays, Salway & Busby, 2005) and mice ( $\sim 300 \mu\text{m}$ ) (Petersen & Crochet, 2013), which is expressed by magnified neurons (total dendritic length ( $\mu\text{m}$ ) of 14,533 in human vs. 5317 in mice and 5128 (Meyer et al., 2010) or 7782 (Narayanan et al., 2015) in rats). These differences raise a question about the similarity in the commonality of PyrNs morphology and whether there is a fixed relationship which is well-preserved over the geometry of the dendritic and axonal neurites of these cells in different mammals.

## **2. Research Goals**

This research was designed to address PyrNs variability in L2/3. We focused on the neuroanatomical differences and their relation to SSP. The distribution of PyrNs neuroanatomy and its relation to the rate of SSP will enable us to define an algorithm which would describe this circuit. Defining a set of functions based on the neuroanatomy and rates of SSP of the PyrNs in this layer would give us the capability to predict those parameters on another PyrNs in this specific brain region and may be expanded to other brain areas, layers and species.

This is the first time that SSP and neuroanatomy are measured by time lapse *in vivo* imaging concomitantly which enable us to relate one to the other. Furthermore, when compared with other studies whose neuroanatomy analysis was performed by *in vitro* imaging, our data collection method has a lot of advantages over *in vitro* imaging in slices, although we lose resolution in z axis (2P PSF of ~0.25  $\mu\text{m}$  in the x and y-axis and ~2  $\mu\text{m}$  in the z-axis (~0.4  $\mu\text{m}$  of 1P confocal imaging)); there is no need to perform stitching of the cells, there is no shrinkage or deformation of the cells and we have the possibility to perform time lapse imaging. However, the loss of resolution in the z-axis prevents our ability to extract parameters associated with neurites volume.

We hope such detailed description would be a useful tool for other researchers who investigate L2/3 circuits, and hopefully it could be utilized by researchers who investigate other brain circuits, real and\or artificial.

### **3. Hypothesis**

Since L2/3 is a major hub for information flowing from, within and to many other cortical and subcortical areas in the brain, we assume that we will find a heterogeneous population of PyrNs in this layer. This heterogeneity should be manifested as various neuroanatomy values as well as different rate of SSP. Alternatively, we might find a continued distribution of parameters describing this neuronal population with no distinct subtypes. L2/3 is a thick (~250 micrometer) layer with a gradient of inputs of varying strength from multiple sources, therefore we hypothesize that some cell's parameters will vary in relation to others and could be described as a mathematical function. One specific hypothesis pertains to the rate of spine turnover on distal AD in L1 vs distal BD spine turnover rate deeper in the neocortex. Since input varies by depth, we assume that SSP would be correlated with dendrite type (apical vs basal) and its depth within the AC. Our study will enable us to relate cell neuroanatomy to the rates of its SSP (of pre-synaptic; axonal boutons and post-synaptic; apical and basal dendritic spines) thus relating, for the first time, these parameters to each other within a particular neuron. Moreover, this unique mathematical description could be used for predicting and testing for a possible common 'blueprint' of PyrNs in other cortical layers, brain structures and other mammalian species.

## **4. Materials and Methods**

### **4.1. Surgical Procedures**

All experimental procedures used in this study were approved by University of Haifa Animal Care and Use Committee. Female CBA/CaJ mice ( $n = 47$ , 7 weeks old) were anesthetized in all imaging sessions using fentanyl-based anesthesia. Rectal temperature was maintained at  $36 \pm 1$  °C and monitored continuously. A metal pin was glued to the skull, using dental cement and then connected to a custom stage, to allow precise positioning and repositioning of the head during the time-lapse imaging sessions. A small opening (3 mm diameter) was made with a drill over the left hemisphere barrel field to accommodate insertion of the glass pipette through one or two separate penetration points (2.5 to -3 mm lateral to the midline, 1–1.5 mm posterior to bregma, -0.25 to -0.45 mm from the brain surface). Chronic windows were implanted based on an established preparation (Cohen and Bonhoeffer, unpublished). Following surgery animals returned to the animal facility for recovery. At the end of experiments, animals are sacrificed with an overdose of sodium pentobarbital.

### **4.2. Electrophysiology and Electroporation**

Cell-attached recordings were obtained using blind/targeted patch-clamp recordings. Electrodes (7–10 MΩ) were pulled from filamented, thin-walled borosilicate glass (outer diameter, 1.5 mm; inner diameter, 1.0 mm; Hilgenberg). The internal solution contained 140 mM K-gluconate, 10 mM KCl, 10 mM Hepes, 10 mM Na<sub>2</sub>-phosphocreatine, 4 mM MgATP, 0.4 mM Na<sub>2</sub>GTP, and 0.5 mM EGTA, and was adjusted to pH 7.25 with KOH. The internal solution also contained 0.2 µg/µL plasmid DNA (driving GFP expression under a CAG promoter).

A custom-made relay configuration allowed us to toggle between electrical recording and electroporation using the same electrode. The double-pole, double-throw relay (DPDT basic relay; Teledyne Relays) served two functions. First, it allowed us to switch between an amplifier configuration for recording the small currents generated by spikes and a high-voltage source configuration for DNA electroporation using large currents. Second, by grounding the head-stage amplifier during electroporation, we protected the amplifier's input and minimized the period needed to reestablish the recording session.

Electroporation Parameters: Between 50 and 80 square 1–2 µA (10–20 V) pulses of 0.5-ms duration at a frequency of 50 Hz were effective for electroporation. The electroporation

parameters were optimized for each cell by changing the injected current amplitude, following a calculation of the effective negative voltage in the range of 20–40 V [(pipette resistance + membrane seal resistance)  $\times$  injected current = effective voltage]

#### **4.3. Imaging**

In vivo two-photon imaging was carried out on an Olympus FV1000BX61 system equipped with a mode-locked Ti:sapphire laser (Mai Tai DeepSee, Spectra-Physics) through a 25x water immersion objective (1.05 NA, Olympus). Laser settings and image acquisition were controlled by Fluoview software (Olympus). For structural *in vivo* imaging mice were anaesthetized with fentanyl-based anesthesia and placed on a feedback controlled heating pad. Data was acquired at 940 nm with an average laser power of <30 mW, and the emission signal was directed through a dichroic mirror (DM570) and red/green band pass emission filters (BA495-540HQ and BA570-625HQ, all Olympus); a typical imaging session lasted 2 h. Mice were imaged as early as 10 days post-surgery. Individual electroporated cells were identified and followed imaged again with intervals of 9 days (2-10 sessions). In the first imaging, session high-resolution tiled volume stacks (510 x 510  $\mu$ m field of view; 0.49 $\mu$ m/px; 2-5 $\mu$ m z-steps) were acquired up to a depth of 450  $\mu$ m from the pial surface for overview and reconstruction of whole cell morphology of labeled cells. In addition, high resolution close-up stacks (73 x 73  $\mu$ m; 0.14  $\mu$ m/px; 1  $\mu$ m z-steps) of typical 6-10 individual dendritic and axonal processes were acquired at various depths between 20 and 350  $\mu$ m.

#### **4.4. Analysis of *in vivo* structural data**

Image stacks were processed using the Fiji package of ImageJ (US National Institutes of Health) as follows: Images were converted to 8 bit and subjected to a small 2D Median filter ( $\sigma < 0.6$  px). For display purposes only, maximum intensity z-projections are shown with adjusted brightness/contrast.

Whole cell morphology was reconstructed using FIJI Simple Neurite Tracer (<https://fiji.sc/>). Briefly, AD and BDs were semi-automatically traced through the high-resolution tiled volume stack. The SWC file of the reconstructed cells was imported to Python and the following parameters were extracted and/or calculated for each cell using a custom written code (Figure 2).

In order to determine spine and bouton densities, dynamics and survival, putative synaptic structures were identified in image stacks at each recorded time point. We included all clearly visible structures in x and y. An ID was assigned to each individual identified structure at the time point of its first appearance and registered across time points (the procedure of pre-processing is described in figure 2). Density is reported as structures per  $\mu\text{m}$ , gain and lost are calculated as fraction of structures (gained or lost<sub>t2</sub>) / total<sub>t1</sub> and turnover is calculated as fraction of structures (gained<sub>t2</sub> + lost<sub>t2</sub>) / (total<sub>t1</sub> + total<sub>t2</sub>).

Synaptic Plasticity Pre-processing:

1. Opening the stack image (basal/apical dendrite or axon) in Fiji.
2. Subtracting red channel from green channel.
3. Running a one pixel median filter to smooth the image appearance.
4. Registration to correct specimen movements during acquisition
5. Brightness & contrast correction
6. Choosing the relevant slides from the stack and performing Z project.
7. FFT algorithm of band-pass filter.
8. Inverting LUT.
9. Background subtraction.
10. Adjusting brightness and contrast.
11. Repeating all the steps for stacks of all time points.
12. Opening all time points finalized images and collapsing them onto one stack.
13. Converged stack registration to align all images
14. Cutting the irrelevant edges and breaking the stack back to isolated images.
15. Inserting the images into a slide on Power Point according to chronological order.
16. Pre- and post-synaptic structures annotation by arrows.
17. Synaptic plasticity analysis with Excel.

Neuroanatomy Pre-processing:

1. Opening stack in Fiji.
2. Subtracting red channel from green channel.
3. Registration to correct specimen movements during acquisition
4. Brightness & contrast correction
5. Opening Simple Neurite Tracer plugin for reconstruction.
6. Tracing all basal dendrites.
7. Tracing the apical dendrite.
8. Tracing the axon.
9. Tracing the soma.
10. Converting and exporting all the traces as SWC files.
11. Neuroanatomical analysis of the SWC files with custom written Python code.

**Figure 2: Data pre-processing flowchart.** Chronological stages of data pre-processing

## 5. Results

Our data was acquired in the left hemisphere AC of female CBA/CaJ mice. This dataset was acquired at the MPI in Munich at the department of prof. Tobias Bonhoeffer by Dr. Cohen Lior using *in vivo* two-photon imaging (see methods). Animals were imaged every nine days for 2-10 sessions in total.

In order to improve data quality and to increase signal to noise ratio we employed several preprocessing image steps using Fiji software (<https://fiji.sc/>) prior to anatomical analysis. Our database consists of 67 cells and their average sub-pial depth is  $196 \pm 57.59 \mu\text{m}$  (mean  $\pm$  std) thus sampling the entire mouse L2/3 (Watson & Paxinos, 2010).

### 5.1. Data processing:

For SSP image preprocessing (Figure 2a) we opened a zoom in z-stack of an AX or a dendrite section in Fiji. Since the data was acquired under red/green band pass emission filters, we subtracted the red channel from the green channel in order to reduce background noise (Figure 3a-c). In the next step, we ran one-pixel median filter as described in figure 3d. Next, we ran a registration algorithm to correct for mouse movements during acquisition (Figure 3e). We chose the relevant slides from the stack and performed Z projection in order to view the whole image in two dimensions. In order to further sharpen the image, we utilized an FFT algorithm of band pass filter followed by inversion of LUT for better visualization (Figure 3f and g). Next, we subtracted the background and adjusted the brightness & contrast to achieve clear appearance (Figure 3h). We repeated all steps several times for each imaging time point, and then we merged all final images into one chronological time-series. As shown in figure 3i the images from different time points are not perfectly align, therefore, we preformed another registration on this chronological time-series to align the time lapse images (Figure 3j). To prepare the processed data for annotation we cut the irrelevant edges of the images and broke the time-series back to isolate chronological images. These final processed images were inserted by chronological order into a Power Point slide for further manual annotation of pro- and pre-synaptic structures (Figure 3k). The arrows were colored with four different colors. The blue arrows were assigned to synaptic structures that were stable over the course of the experiment, green arrows were assigned to new synaptic structures, red arrows to synaptic structures that disappeared and yellow arrows to synaptic structures who were stable before they disappeared or after they appeared. The different colored arrows were quantified and spine\bouton density, gain, loss and turnover rates were calculated.

For images of cells neuroanatomy preprocessing (Figure 2b) we opened a cell z-stack on Fiji, subtracted red channel from green channel (Figure 4a-c) and ran registration to correct mouse movement during data acquisition. Next, we opened Simple Neurite Tracer plugin for cell reconstruction (Figure 4d). We traced all of the cell neurites. First, we traced the soma and labeled the trace as 'soma'. Second, we traced and labeled the BDs that descend from the base and the apex of the soma. Next, we traced and labeled the AD which ascends from the apex of soma toward the surface and finally we traced and labeled the AX that descends from the base of the soma downward splitting and diverging in every possible direction. When the entire neuron was traced, we visualized it on 3D (see all traces in figure 4d-e). Then, we converted and exported all the traces as SWC files, which were used for neuroanatomical analysis, using a custom written python code.

It is important to note that all annotation, reconstruction and extraction of further parameters followed a double-blind procedure.

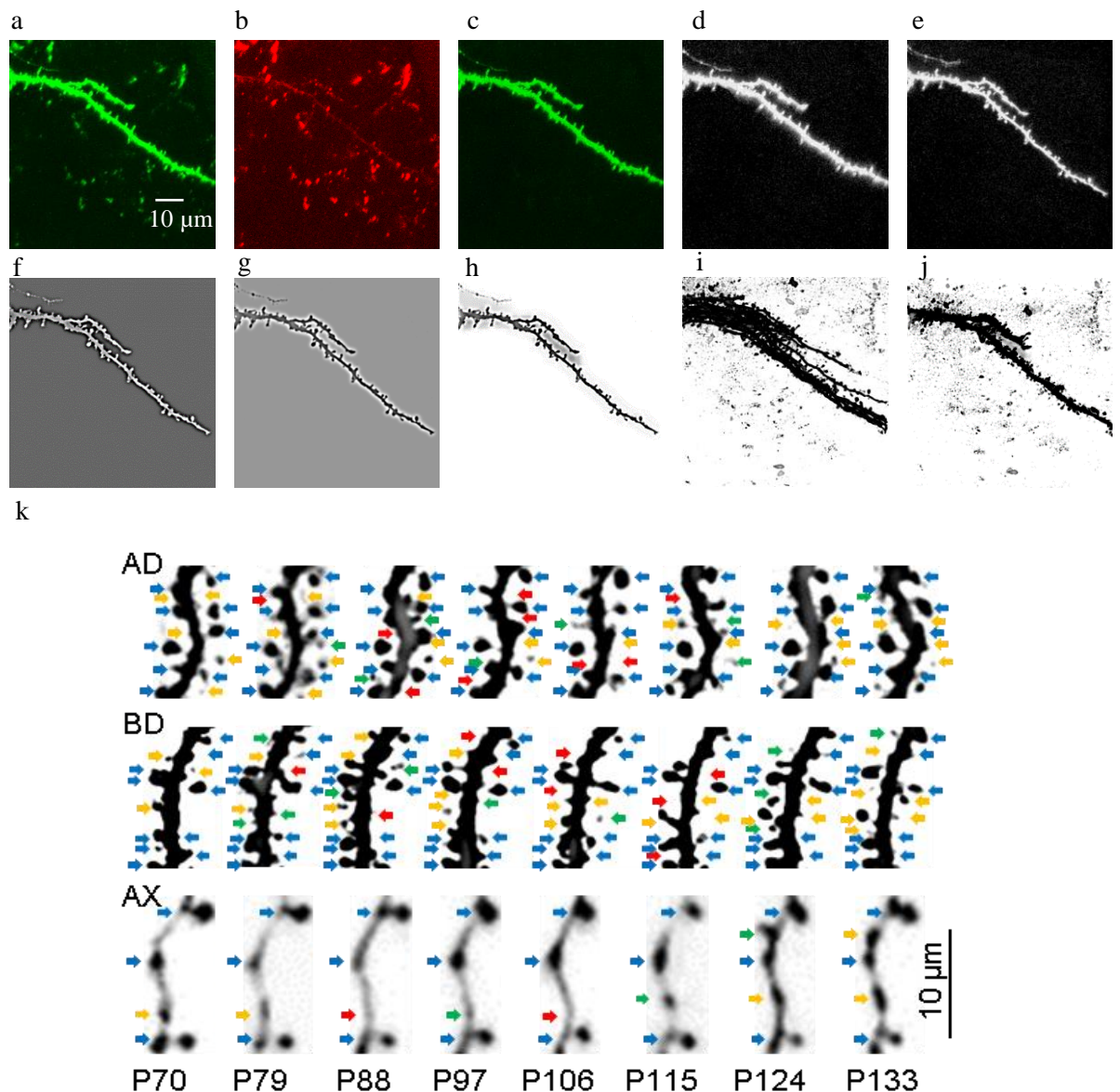


**Figure 3: Synaptic plasticity pre-processing.**

An example of BD pre-processing. a to c. Subtraction (c) of the red channel (b) from the green channel (a). d. Image after one pixel median filter. e. Image after registration. f. Image after z project and fast fourier transform algorithm of band pass filter. g. Image after inverting the LUT. h. Image after background subtraction. i. Image after pre-processing a-h, from nine time points. The image is a z project of all the time points. j. Z project of nine time points which aligned after registration. k. An example of arrows annotation. The bottom line represents number of days of the mouse's life in each time point. Spines\boutons that were stable over time represented by blue arrows, new spines\boutons by green arrows, spines\boutons that were disappeared represented by red arrows and spines\boutons that were stable but not over the all experiment time represented by yellow.

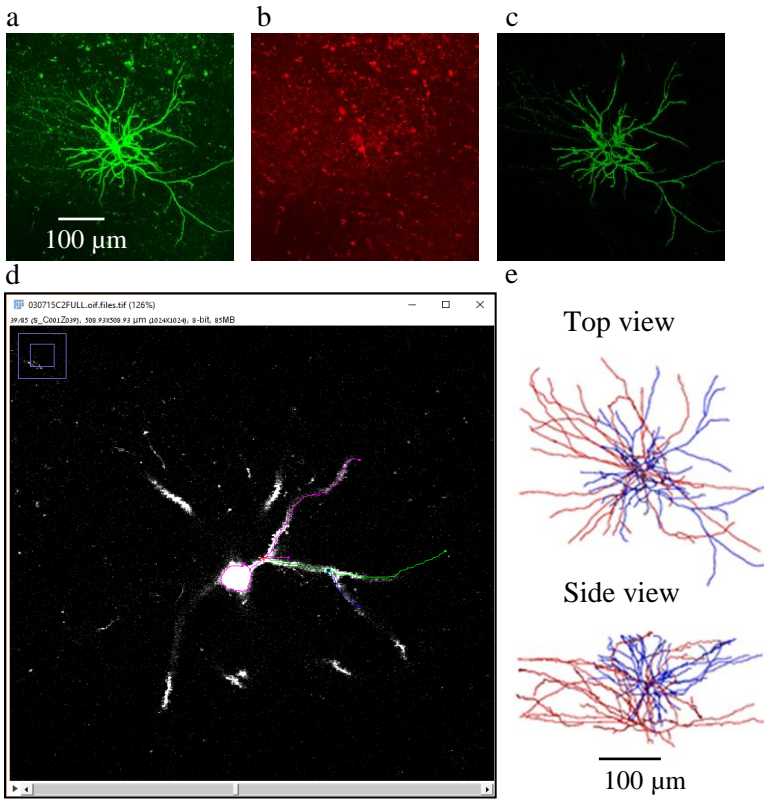


**Figure 4: Neuroanatomy pre-processing.**

An example of pyramidal neuron pre-processing. a-c. Subtraction (c) of the red channel (b) from the green channel (a). d. Image reconstruction in Simple Neurite Tracer plugin. e. Top view and side view following reconstruction. The dendrites represented by blue and the AXs by red.

## 5.2. Parameters extraction and validation:

For neuroanatomy and SSP analysis we extracted and calculated the following parameters listed below. In this list, every parameter has a key number which represents this parameter in all following figures:

1. **Soma depth** – The depth of the soma, measured from the superficial surface,  $\mu\text{m}$ .

### Synaptic structures

2. **BDs spine density** – The number of spines per one  $\mu\text{m}$ ,  $n/\mu\text{m}$ .

3. **BDs spine turnover** – The average percent of spines that were gained\lost over time ( $\Delta t= 9$  days), calculated by  $(\text{gain} (\%) + \text{lost} (\%))/2$ , %.

4. **ADs spine density** - The number of spines per one  $\mu\text{m}$ ,  $n/\mu\text{m}$ .

5. **ADs spine turnover** - The average percent spines that were gained\lost over time ( $\Delta t= 9$  days), calculated by  $(\text{gain} (\%) + \text{lost} (\%))/2$ , %.

6. **Axonal boutons density** - The number of boutons per one  $\mu\text{m}$ ,  $n/\mu\text{m}$ .

7. **Axonal boutons turnover** - The average percent boutons that were gained\lost over time ( $\Delta t= 9$  days), calculated by  $(\text{gain} (\%) + \text{lost} (\%))/2$ , %.

### Apical dendrite

8. **Bifurcations** - Counts the number of branching points with only 2 children, n.

9. **Forking points** - Counts the number of branching points with two or more children, n.

10. **Sections** - Number of sections, n. (A section is a tree node containing a series of two or more points whose first and last element are any of the following combinations: 1. Root node, forking point 2. Forking point, forking point 3. Forking point, endpoint 4. Root node, endpoint)

11. **Terminations** - Number of endpoints, n.

12. **Total length** - Gets the total length of all sections,  $\mu\text{m}$ .

13. **Post synaptic spine number** – Calculates the number of spines by multiplying the density with the total length of the neurite, n.

14. **Principal direction extents (mean)** - The major direction vector (The extent is defined as the maximum distance between the projections on the principal directions of the covariance matrix of the points),  $\mu\text{m}$ .

15. **Remote bifurcation angles (mean)** - Gets a list of the angles between branches in a fork point by their endpoints, rad.

16. **Section branch orders (mean)** - Gets a list of the number of branches at any bifurcation, starting from the soma (value 0) toward to the endpoints, n.

17. **Section lengths** - Mean section lengths,  $\mu\text{m}$ .

18. **Section path distances** - The mean of the distance of the path from the soma to the section,  $\mu\text{m}$ .

19. **Section radial distances** - Gets the mean of the distance from the soma for all sections,  $\mu\text{m}$ .

20. **Apical Dendrite type** – AD type: 0) 1 AD. 1) 1 normal AD. 2) 2 ADs. 3) No AD, n.

### **Basal dendrites**

21. **Bifurcations** - Counts the number of branching points with only 2 children, n.

22. **Forking points** - Counts the number of branching points with two or more children, n.

23. **Sections** - Number of sections, n.

24. **Terminations** - Number of endpoints, n.

25. **Total length** - Gets the total length of all sections,  $\mu\text{m}$ .

26. **Post synaptic spine number** - Calculates the number of spines by multiplying the density with the total length of the neurite, n.

27. **Principal direction extents (mean)** - The major direction vector,  $\mu\text{m}$ .

28. **Remote bifurcation angles (mean)** - Gest a list of the angles between branches in a fork point by their endpoints, rad.

29. **Section branch orders (mean)** - Gets a list of the number of branches at any bifurcation, starting from the soma (value 0) toward to the endpoints, n.

30. **Section lengths** - Mean section lengths,  $\mu\text{m}$ .

31. **Section path distances** - The mean of the distance of the path from the soma to the section,  $\mu\text{m}$ .
32. **Section radial distances** - Gets the mean of the distance from the soma for all sections,  $\mu\text{m}$ .
33. **Basal neurites** - Number of basal neurites in a neuron, n. (A neurite is a primary tree that comes out from the soma).
34. **Neurite lengths** - Gets the mean of path length per basal neurite,  $\mu\text{m}$ .
35. **Sections per neurite** - Gets the mean number of sections per neurite in a collection of basal neurites, n.

### Axon

36. **Bifurcations** - Counts the number of branching points with only 2 children, n.
37. **Forking points** - Counts the number of branching points with two or more children, n.
38. **Sections** - Number of sections, n.
39. **Terminations** - Number of endpoints, n.
40. **Total length** - Gets the total length of all sections,  $\mu\text{m}/0.1\text{mm}^3$  (relating to the averaged sampled cortical volume).
41. **Pre synaptic bouton number** - Calculates the number of boutons by multiplying the density with the total length of the neurite, n.
42. **Principal direction extents (mean)** - The major direction vector,  $\mu\text{m}$ .
43. **Remote bifurcation angles (mean)** - Gets a list of the angles between branches in a fork point by their endpoints, rad.
44. **Section branch orders (mean)** - Gets a list of the number of branches at any bifurcation, starting from the soma (value 0) toward to the endpoints, n.
45. **Section lengths** - Mean section lengths,  $\mu\text{m}$ .
46. **Section path distances** - The mean of the distance of the path from the soma to the section,  $\mu\text{m}$ .
47. **Section radial distances** - Gets the mean of the distance from the soma for all sections,  $\mu\text{m}$ .

### Sum of all neurites

48. **Bifurcations** - Counts the number of branching points with only 2 children, n.
49. **Forking points** - Counts the number of branching points with two or more children, n.
50. **Sections** - Number of sections, n.
51. **Terminations** - Number of endpoints, n.
52. **Total length** - Gets the total length of all sections,  $\mu\text{m}$ .
53. **Principal direction extents (mean)** - The major direction vector,  $\mu\text{m}$ .

54. **Remote bifurcation angles (mean)** - Gets a list of the angles between branches in a fork point by their endpoints, rad.
55. **Section branch orders (mean)** - Gets a list of the number of branches at any bifurcation, starting from the soma (value 0) toward to the endpoints, n.
56. **Section lengths** - Mean section lengths,  $\mu\text{m}$ .
57. **Section path distances** - The mean of the distance of the path from the soma to the section,  $\mu\text{m}$ .
58. **Section radial distances** - Gets the mean of the distance from the soma for all sections,  $\mu\text{m}$ .
59. **All neurites** - Number of neurites, n.

First, we compared synaptic structure density and turnover rate between the three types of neurite's segments we have sampled (AD, BD and AX) (Figure 5). We found that AX boutons density ( $0.29 \text{ n}/\mu\text{m}$ ) is significantly lower compared to apical ( $1.15 \text{ n}/\mu\text{m}$ ) and basal ( $1.22 \text{ n}/\mu\text{m}$ ) dendrites spines density ( $P<0.001$ ) as described in previous studies (De Paola et al., 2006). In addition, we found that spines turnover rate of BD ( $10.1\%$ ) is significantly lower compared to those of AX ( $13.9\%$ ), AD ( $13.7\%$ ) ( $p<0.001$ ).

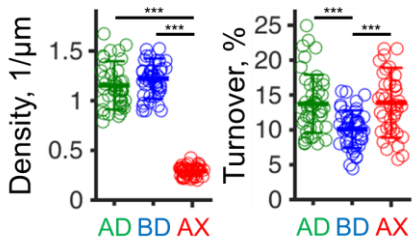


**Figure 5: Synaptic structure neurite types comparing.**

Comparison of mean values of density (left panel) and turnover rate (right panel) between AD (green), BD (blue) and AX (red). X axis represents neurite type and Y axis the value. The scale bar in each dot represents the mean $\pm$ std. Astrisks indicate T-TEST significance level.

After we extracted all possible parameters for each cell, we have calculated the mean value and its distribution. First step was to examine the validity of our data, since there could be no significance for such results if a neuron's neurite anatomy changes over time. To test for possible alteration of PyrNs neuroanatomy over time we imaged and subsequently reconstructed 15 cells ,each cell twice, over two months interval and compared their neuroanatomy. Out of these 15 cells we identified only two cells, which altered their neurite anatomy over time (Figure 6). These changes were small ( $5\text{-}20 \mu\text{m}$ ) and restricted to terminal sections. The cell in figure 6b gained extra small terminal branch on his AD. The second PyrN (Figure 6c) lost two small terminal branches on his AX and one terminal branch on his AD over time. Thus, the neuroanatomy of PyrNs in adult mammals is highly stable.

Since the depth at which we can look into the cortex is limited, we had to rule out the possibility that our results could be biased due to diminishing optical access deeper in the AC.

We found a series of results assuring us this have not been the case (Figure 7, Table 1). First, if the measurement were noisy deeper in the AC, we would expect finding a higher distribution of parameters and more correlations related to imaging depth. However, we found that only BD spines density was varied depending on the section's depth ( $r=-0.34$ ,  $p<0.001$ ), while AD's and AX's densities were not (Table 1, section depth). Hence, BD spines density is negatively correlated to dendrite section position within AC L2/3. Independently, we found that the AD spines turnover is negatively correlated with section's depth ( $r=-0.34$ ,  $p<0.001$ ), while the BD spines turnover rate tends to be positively correlated to section's depth ( $r=0.18$ ,  $p=0.08$ ). In addition, we found a negative correlation between soma depth and BD spines density ( $r=-0.38$ ,  $p=0.0001$ ), which was expected as the depth of basal sections is similar to that of the soma. As well as a negative correlation between soma depth and AD spine density ( $r=-0.33$ ,  $p<0.001$ ). We did not identify any significant correlations between axonal boutons and cortical imaging depth. Together these results indicate that, first, there is no bias due to imaging depth; second, there is an intricate synaptic connectivity pattern which is closely related to soma depth and section type and depth which is probably governs by the input afferent pattern in the AC.

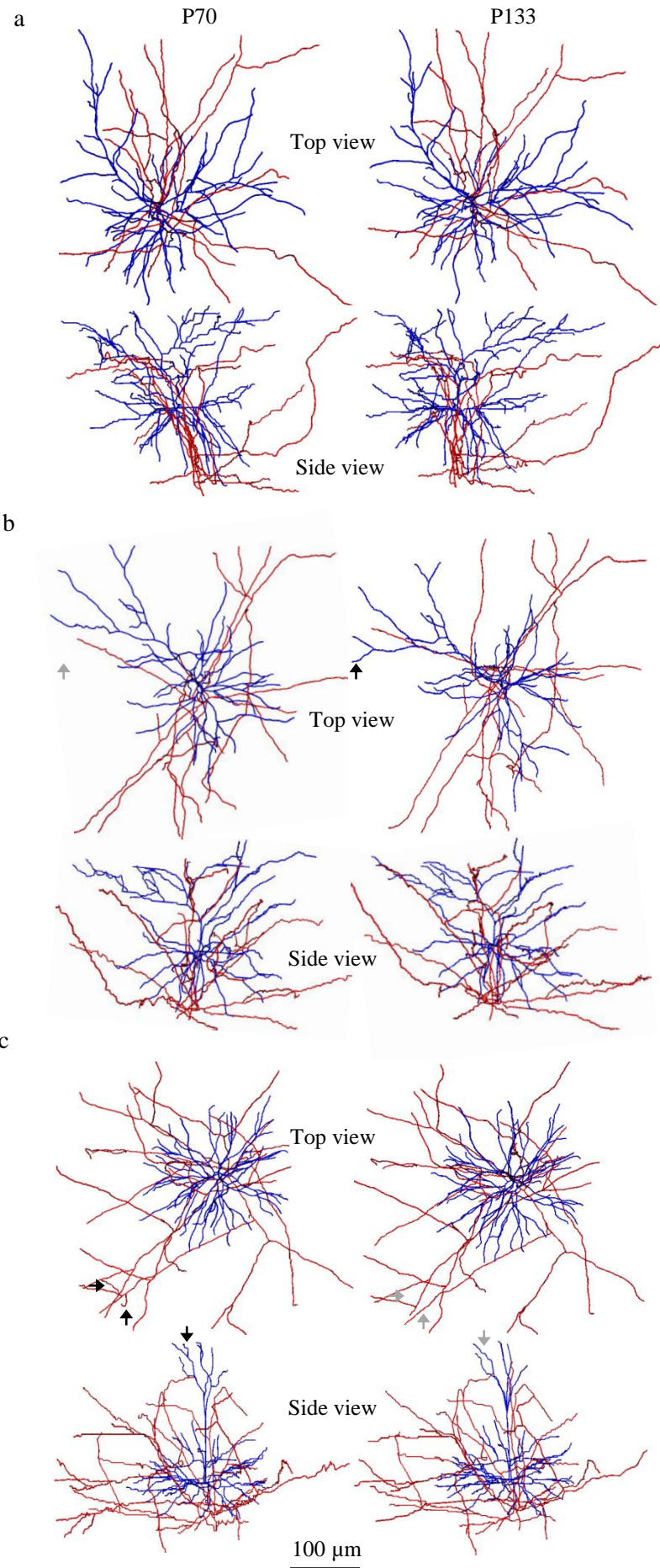


**Figure 6: Two time points, reconstruction comparisons.**

Examples of three neurons reconstructions two months apart. Dendrites represented by blue, AXs by red. a. Top view and side view of neuron with no differences between time lapse reconstructions. b. Top view and side view of neuron with extra branch point in the AD (represented by black and gray arrows) compared to time point No. two. c. Top view and side view with two extra branch points in the AX's and one in the AD's trees (represented by black and gray arrows).

**Table 1: Synaptic plasticity correlations.**

	<b>Soma depth</b>	<b>Section depth</b>	<b>Section distance</b>
AD spines turnover	$r=0.13, p=0.2$ n=98	$r= -0.34, p=0.0006$ n=98	$r = 0.1, p=0.34$ n=98
AD spines density	$r= -0.33, p=0.0008$ n=101	$r=0.06, p=0.5$ n=101	$r = -0.03, p=0.78$ n=101
BD spines turnover	$r=0.16, p=0.1$ n=93	$r=0.18, p=0.08$ n=93	$r = 0.1, p=0.43$ n=93
BD spines density	$r= -0.38, p=0.0001$ n=96	$r= -0.34, p=0.0007$ n=95	$r = -0.1, p=0.23$ n=97
AX boutons turnover	$r= -0.18, p=0.1$ n=87	$r=5.1e^{-5}, p=1$ n=79	$r = -0.1, p=0.31$ n=78
AX boutons density	$r=0.18, p=0.1$ n=89	$r=0.26, p=0.8$ n=79	$r = -0.02, p=0.84$ n=78

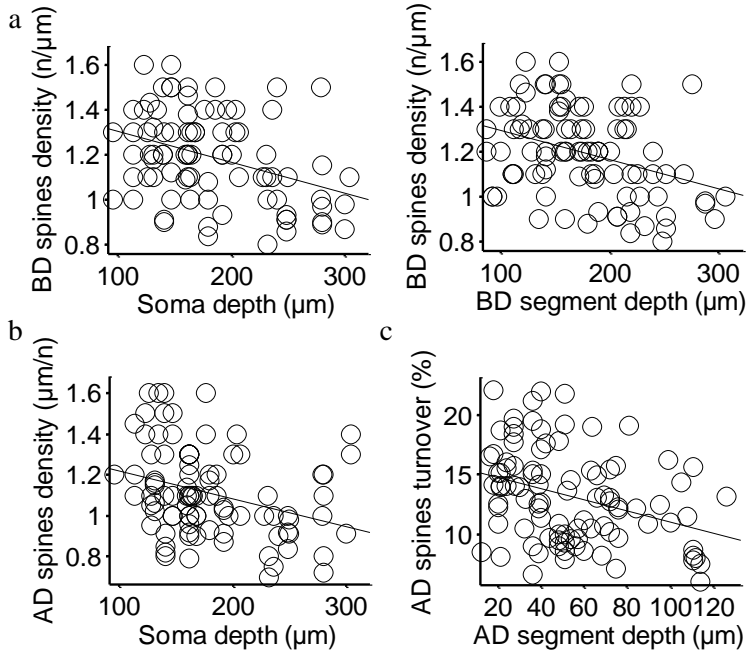


**Figure 7: Correlations between synaptic plasticity and depth.**  
Four significant correlations (n=46 neurons). The dots represent each neuron. Black line- regression line. a. Left; Negative correlations between soma depth and BD spines density, ( $r = -0.35, p<0.001$ ). Right; Negative correlations between BD segment depth and BD spines density ( $r = -0.38, p=0.0001$ ). b. Negative correlation between soma depth, and AD spines density ( $r = -0.33, p<0.001$ ). c. Negative correlation between AD segment depth and AD spines turnover rate, ( $r = -0.34, p<0.001$ ).

### 5.3. Parameter Analysis:

Once we ruled out any possible biases in our dataset acquisition and/or analysis we ran the parameter distribution analysis (Figure 8). As you can see, there are 3-4% outliers ( $>2$  std) in all the parameters and 50% of the points that represent outliers are attributed to five cells (7% of our dataset of 67 neurons). These few cells could explain large part of the variance in our dataset. Moreover, the standard deviation of all parameters is substantially smaller than their mean. Thus, AC L2\3 PyrNs are a relatively homogenous population of cells.

There is a considerable gap between amount of spines vs boutons since we didn't have full reconstruction of PyrNs AX, neither in x and y axes, nor in z axis in which a substantial part of the AX is splitting into L5 (Petersen & Crochet , 2013; Rodney & Kevan, 2004).

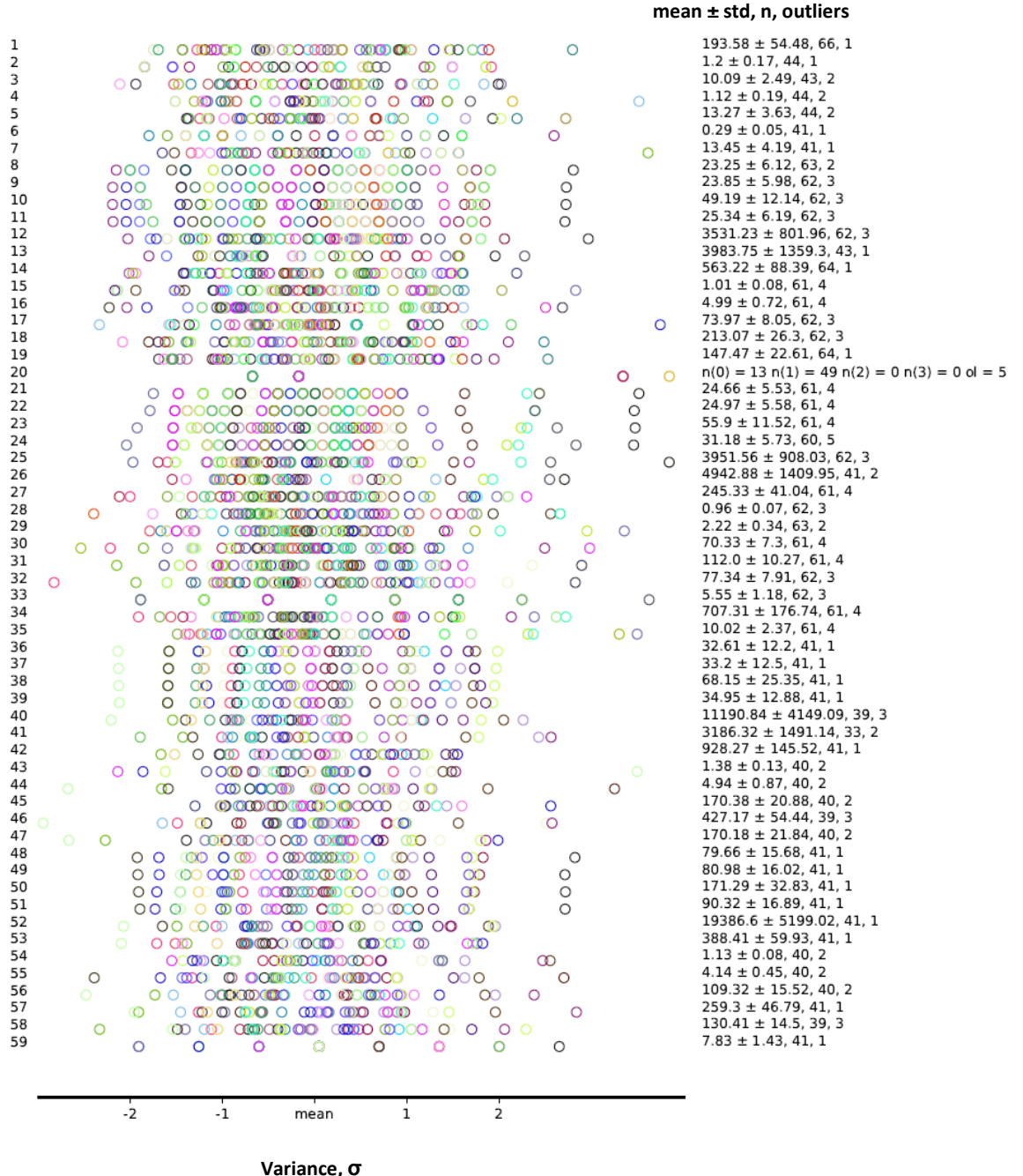


**Figure 8: Parameters distribution.**

Display of distribution for each parameter according to standard deviations normalization. The numbers in the left represent the parameter's key in the 'Parameter List'. Each color across all the parameters represented the results of a single neuron. On the right; information regarding the mean  $\pm$  std, the number of neurons and the number of outliers for each parameter. Parameter No. 20 is a nominal parameter and has only description of the number of neurons in each category.

In addition, we can see in parameter No. 20 (AD type) that most of the cells had one normal AD (49) (Figure 9d), but we were able to find more types of cell's structures. Thirteen cells had one oblique AD. These PyrNs differ in their a/symmetric arborizations (Figure 9c) as was previously reported (Hardingham et al., 2011). PyrNs with oblique AD were found to occupy upper L2/3 (Figure 11l). Four PyrNs have two ADs (Figure 9a and b) and for one cell we could not identify an AD. Some examples are shown in figure 9 and all cells reconstructions are presented in appendix 1.

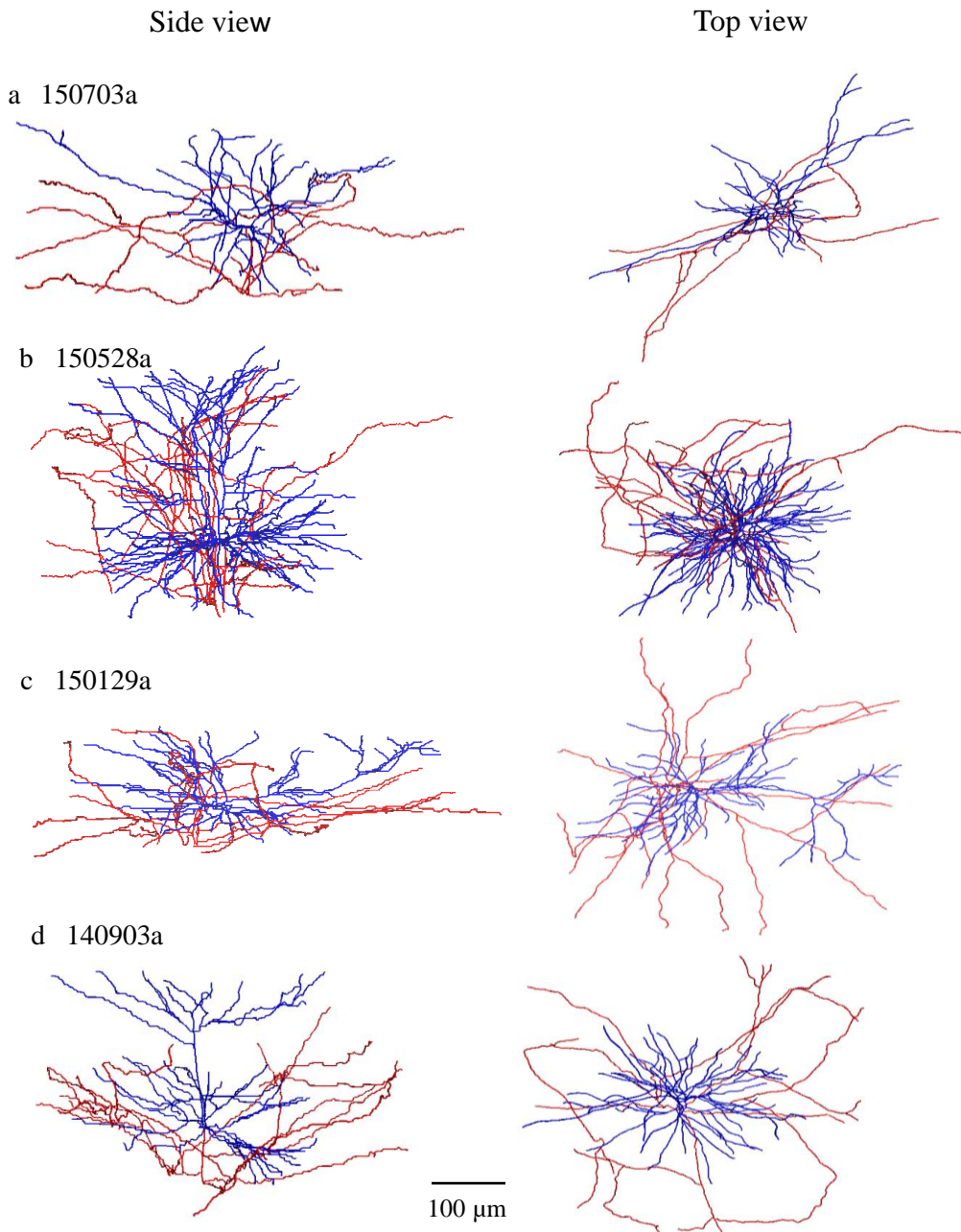


**Figure 9: Different structures of L2/3 PyrNs.**

Side view and top view of four different Types of AD. a. A neuron with two oblique ADs. b. A neuron with two normal ADs. c. A neuron with one oblique AD. d. A neuron with one normal AD.

In order to further describe L2/3 PyrNs population we ran correlation analysis between all possible pairs of parameters (Figure 10). First, we removed from each parameter the outliers that were above 2 std from the mean (Figure 10a and c). In order to check if the correlations we found are real rather than the behavior of different groups in the layer, we also removed outliers that were above 1.5 std from the mean (Figure 10b and d). The correlations we found were preserved independently from the std threshold (with reduced q-values), and hence, reliably represent the neuroanatomy of L2/3 PyrNs (Figure 10). The neuroanatomy parameters were subdivided into five groups: soma depth and SSP (parameters 1-7), AD (8-20), BD (21-35), AX (38-47) and all (all the neurites combined, 48-59). In each group (except for SSP), there were four parameters with very strong correlation between them ( $r>0.8$ ,  $q<0.1e^{-10}$ ) as they reflect the closely geometrically related attributes of the neurite. These parameters are: 1. Number of bifurcations 2. Number of forking points 3. Number of sections 4. Number of terminations, which all describe the complexity of a neurite tree anatomy. The significant correlations that were unexpected are correlations between parameters of the five groups describing PyrNs neuroanatomy and SSP. In case we identified such correlations with parameters from the four correlated parameters above, we mentioned only one of them, since all others are redundant.

Because we made multiple comparisons (about 1700) between all possible pairs of parameters, we needed to rule out false detection (Type 1 error). Hence, we ran FDR correction, in which q value represented the proportion of false discoveries among all the discoveries (rejections of the null hypothesis). We defined the significant correlations with a high threshold of  $q<0.01$ .

We found interesting correlations between soma depth and neuroanatomy features (Figure 11a-c and l). There were positive correlations between soma depth and section radial distances of ADs ( $r = 0.81$ ,  $q<0.1e^{-10}$ ), soma depth and AD type ( $r=0.4$ ,  $q<0.01$ ) (Not in the figure), soma depth and section radial distances of AXs ( $r=0.54$ ,  $q<0.01$ ), and soma depth with section lengths of BDs ( $r=0.45$ ,  $q<0.01$ ). For SSP parameters we found one correlation (Figure 11d), between apical spine density and basal spine density ( $r=0.5$ ,  $q<0.01$ ). While for the neuroanatomy features, we found many correlations between all the neurites (Figure 11e-h). There were correlations between section radial distances of ADs and total length of BDs ( $r=0.4$ ,  $q<0.01$ ), section radial distances of ADs and section radial distances of AXs ( $r=0.6$ ,  $q<0.001$ ), section lengths of ADs and section radial distances of AXs ( $r=0.5$ ,  $q<0.01$ ), and total length of BDs with section radial distances of AXs ( $0.6$ ,  $q<0.01$ ). Surprisingly, we found strong correlations between SSP and neuroanatomy (Figure 11i-k) – total length of BDs and

presynaptic boutons numbers ( $r = 0.6$ ,  $q < 0.01$ ), total lengths of all the neurites with AD spines turnover rate ( $r=0.6$ ,  $q < 0.01$ ) and number of bifurcations of AXs with AD spines turnover rate ( $r=0.5$ ,  $q=0.013$ ). This is the first time that one could correlate parameter describing a neuron's neuroanatomy, which is stable over time, with parameters describing its SSP which varies over time. Taken together, these results reveal an intricate rule of relation between different anatomical parameters of PyrNs anatomy that could be described within a mathematical function. However, it is unclear whether this unique mathematical description is common to all PyrNs. Thus, we next tested whether we could use our Mouse AC L2\3 PyrNs mathematical function in order to predict and test for a possible common 'blueprint' of PyrNs in different areas, layers and species.

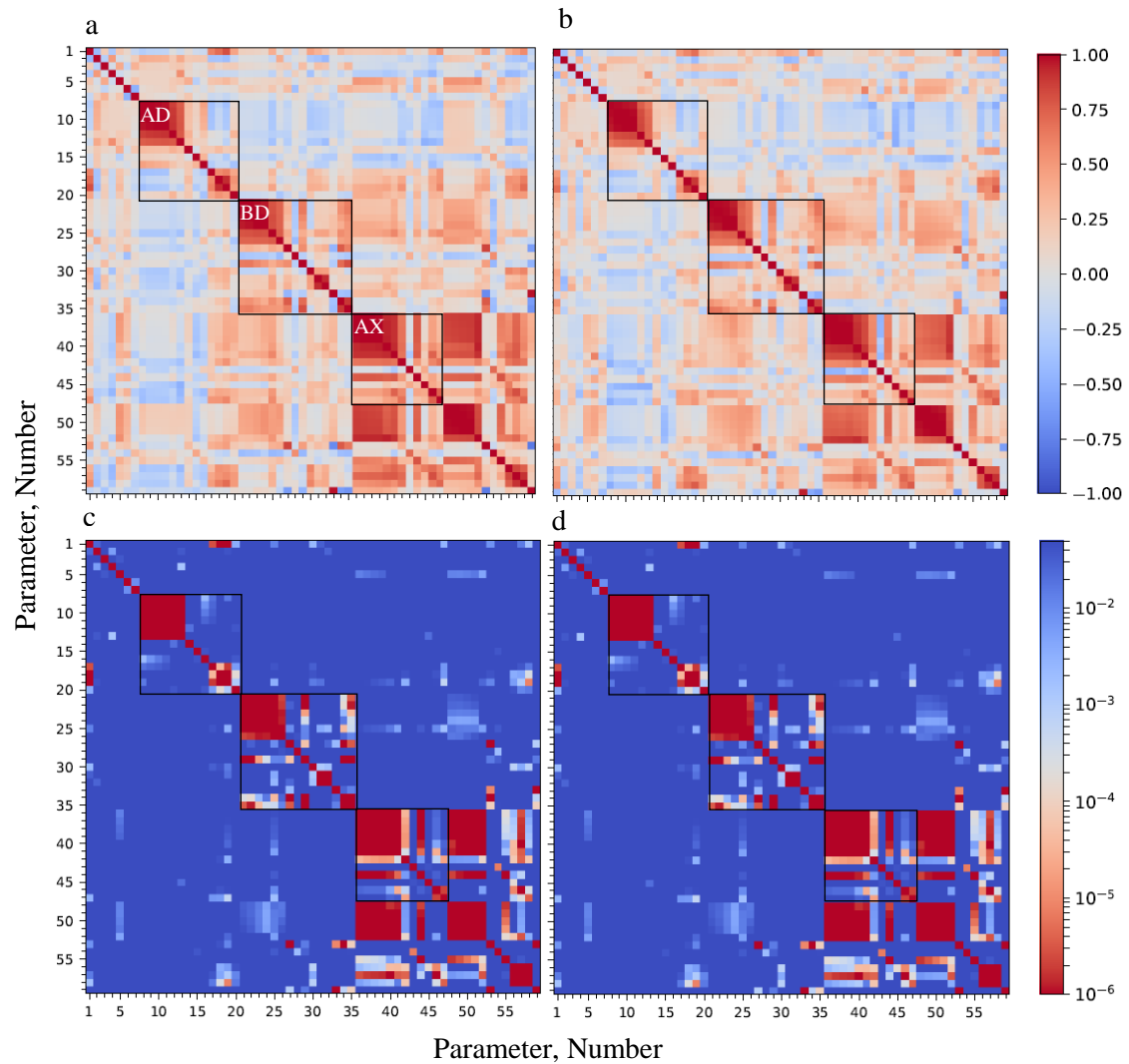


**Figure 10: Correlations color maps.**

Linear correlation and its significance for all possible pairs of parameters. The numbers in the axes represent the number of the parameter and the colors represent the level of the correlation or the significance. a. Correlations between parameters without outliers above 2 std. b. Correlations between parameters without outliers above 1.5 std. c. The significance level (q value) for each correlation we showed in a. d. The significance level (q value) for each correlation we showed in b.

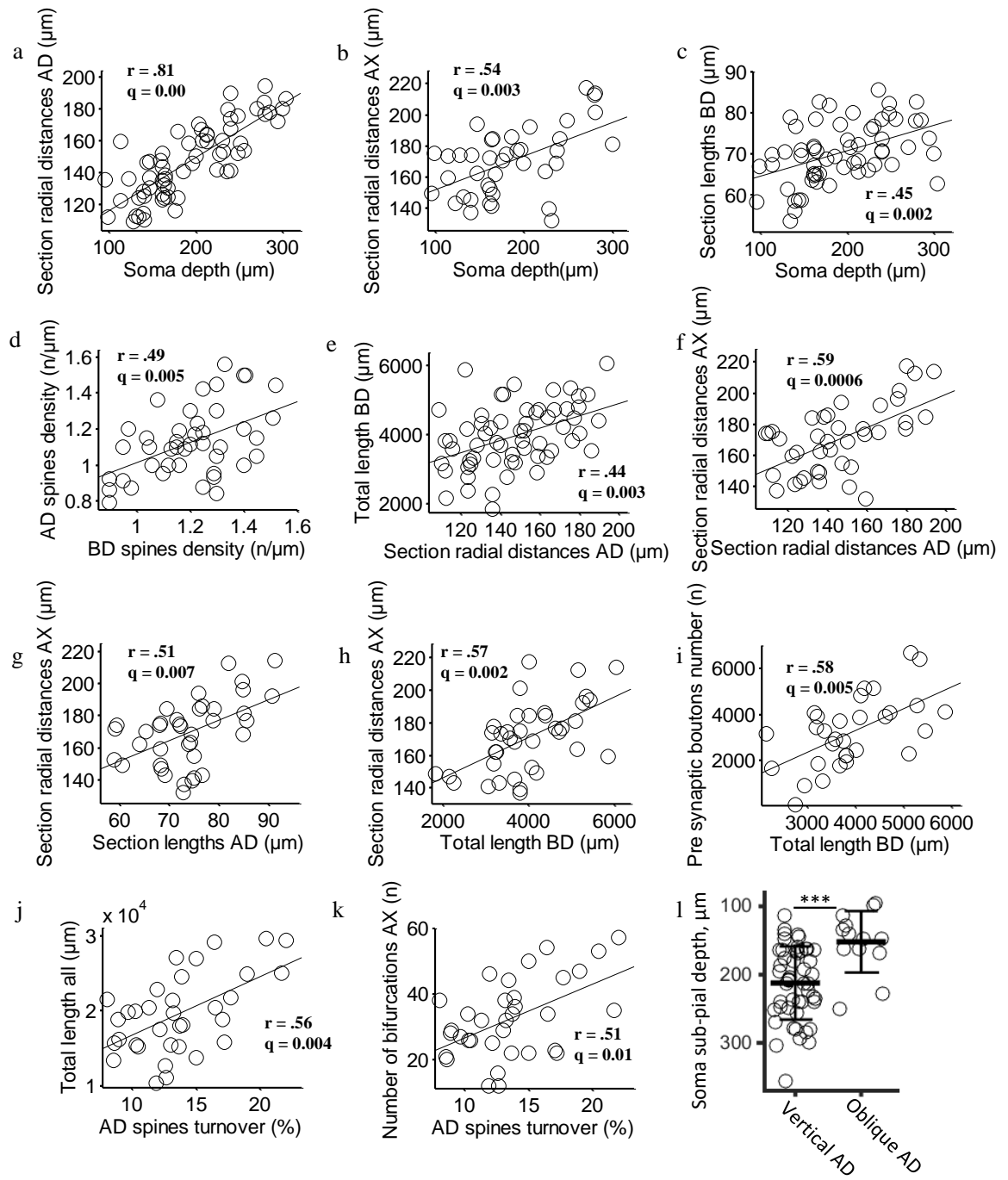


**Figure 11: Linear regression correlations between parameters (a to k).**

$n = 65$  neurons. The dots represent each neuron. Black line - regression line. 1. T-TEST between soma sub-pial depth and AD type. Asterisks indicate T-TEST significance level ( $P < 0.001$ ).

#### **5.4. Preparation of other datasets:**

In order to test for a possible common 'blueprint' of PyrNs in different areas, layers and species based on the rules we have formulated for the mouse AC L2\3 PyrNs, we chose five different other datasets to compare with. The datasets included reconstructed neurons from mouse L2/3 PyrNs, rat L2/3 PyrNs, rat INs, rat L5 PyrNs (were taken from <http://www.neuromorpho.org/>, (Ascoli GA, 2006)), and human L2/3 PyrNs (was taken from Allen Institute for Brain Science, <http://celltypes.brain-map.org/>).

All neuron images were acquired *in vitro* from slices by biocytin staining. Hence, most of the reconstructions had incomplete neurites. In contrast, our dataset images were acquired *in vivo*, and photographed from the top down at a large volume, and hence, had a better quality and more complete neurites trees (all 67 cell in our dataset had complete dendritic neurites imaged and reconstructed). For comparison, we have decided to use only the reconstructions that had SWC file bigger than ~500kb (sizes equal to our smallest size of swc file in our dataset). We applied the file size as a predictor of best reconstructed cell in publicly available datasets. However, due to poor quality of reconstruction of Mouse L2/3 and Rat L2/3 datasets available for us we used files starting from 301kb. Thus, each dataset contained:

Mouse L2/3 – 25/980 files. File size: max: 1.8 Mb min: 301kb average: 531kb median: 385kb

Rat L2/3 – 23/818 files. File size: max: 937kb min: 301kb average: 437kb median: 406kb

Rat L5 – 44/1263 files. File size: max: 5 Mb min: 664kb average: 1.8Mb median: 1.7 Mb

Rat INs – 64/5473 files. File size: max: 3.4 Mb min: 914kb average: 1.3Mb median: 1.1Mb

Human L2/3 – 24/47 files. File size: max: 1 Mb min: 532kb average: 874kb median: 739kb

Our dataset – 65 files. File size: max: 2.1Mb min: 545kb average: 1Mb median: 1 Mb

The mouse dataset was least in number as well as in qualitative reconstructions. There were no other areas or layers with better quality and therefore we took the rat's reconstructions as the main species for comparison. The rat is the most investigated rodent and it has a lot of qualitative data. There are 9434 cell images in neuromorpho when searching the words 'rat' and 'pyramidal' compared to only 5884 with 'mouse'. The rat datasets included neurons mainly from the somatosensory and the visual cortex. The human dataset was sampled from temporal and frontal brain tissues of patients with brain tumors or epilepsy, and the mouse dataset included neurons from the prefrontal, occipital and somatosensory cortex.

Same process of parameters extraction was applied to all datasets, similar to our dataset, via custom written python code, excluding the following parameters which were not

available: soma depth, SSP parameters, AD type and parameters of sum of all neurites that were not necessary for the analysis. The keys numbers in the 'Parameters List' after reducing the parameters we described above are: 8-12, 14-19, 21-25, 27-40 and 42-47. 36 parameters in total.

For each dataset we ran parameters distribution analysis (Figure 12-17). The first thing we found was an unexpected difference between total dendritic length (parameters 12+25) that we found in our dataset ( $7482 \mu\text{m}$ ) compare to mouse PyrNs L2/3 ( $5306 \mu\text{m}$ ) and rat PyrNs L2/3 ( $5081 \mu\text{m}$ ) datasets which should be similar to ours (Figures 12-14). In addition, we found that total length of the neurites in human L2/3 dataset was relatively higher than the other datasets (total length BD  $5831 \pm 3031$  vs  $3954 \pm 908$  in our dataset, or total length AD  $5414 \pm 1636$  vs  $3531 \pm 802$ . Figures 12, 15) while the parameters which present complexity of the neurites was comparable to all other datasets. This is compatible with the thickness of L2/3 in human vs. rat and mouse and with recent fine scale anatomical studies on these neurons which have demonstrated that they are large, in terms of total dendritic length and number of dendritic branches (Mohan et al., 2015; Deitcher et al., 2017).

In rat L5 dataset, we found that most of the AD and AX's parameters which describe complexity and length, had larger mean value compare to our dataset and the other L2/3 PyrNs datasets (for example: number of AD bifurcations  $50.41 \pm 18.51$  vs  $23.25 \pm 6.12$  in our dataset, total AD length  $9796 \pm 1899$  vs  $3531 \pm 802$ ; Figures 12, 16). Rat INs represents completely different type of anatomical blueprint which is manifested as a significantly higher values of AXs parameter's compare to all other PyrNs datasets (number of sections  $664 \pm 351$  vs  $68 \pm 25$  in our dataset (Figures 12 and 17). In addition, it can be seen in rat INs dataset (Figure 17) that there is a larger variance in parameters 21-24 and 35 (std values are almost twice than mean, for example, parameter 21 had substantial range, from 9 to 1837, n) relative to the other datasets which have much smaller variability and the std in all parameters is consistently smaller than the mean. Those differences are presumably due to the heterogeneity that characterized INs group (Moore et al., 2010). This heterogeneity was not identified in our dataset or any of the PyrNs datasets.

## Our dataset

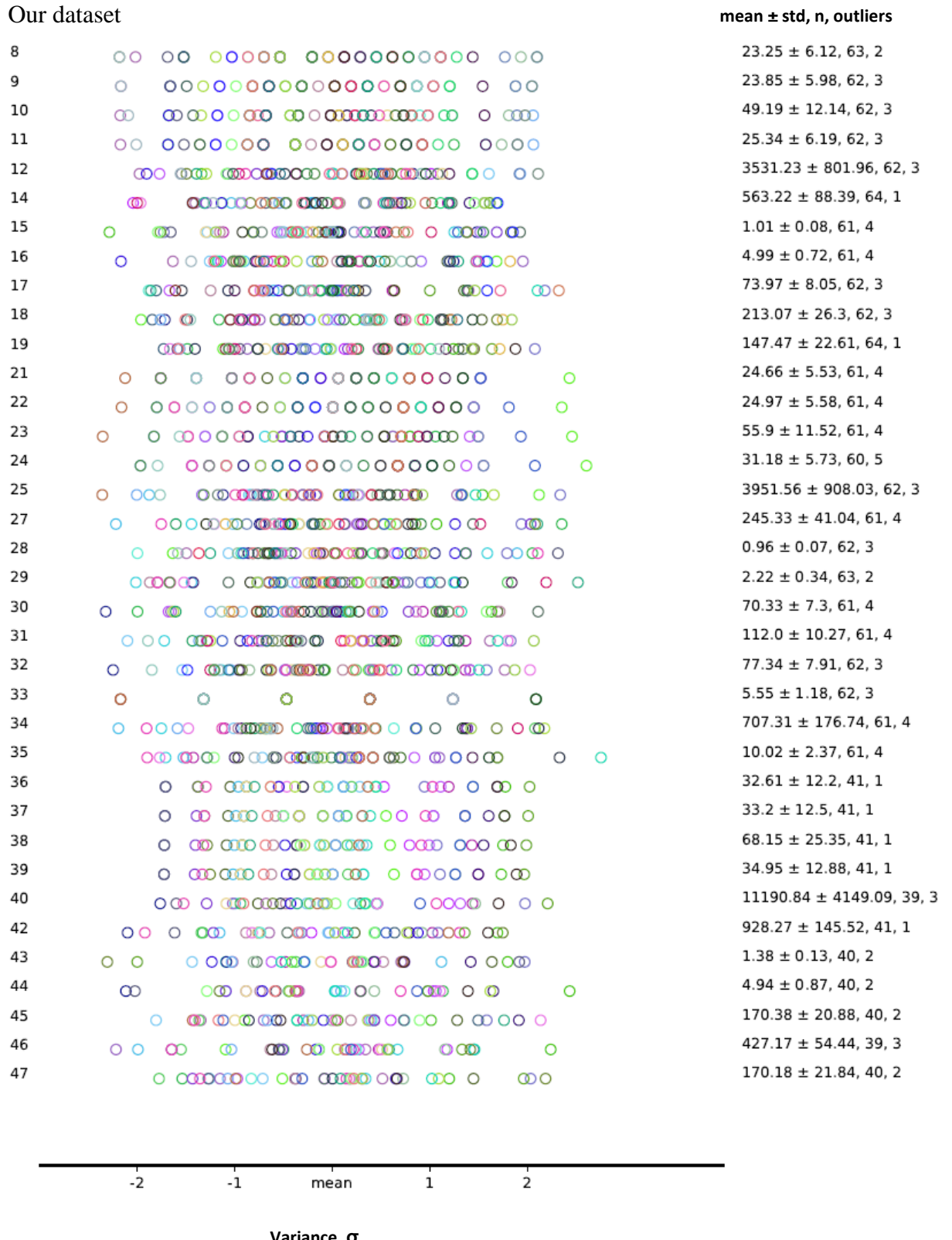


**Figure 12: Our dataset parameters distribution.**

Same data as was shown in figure 8, but only relevant parameters for comparing with other datasets.

## Mouse L2/3

mean  $\pm$  std, n, outliers

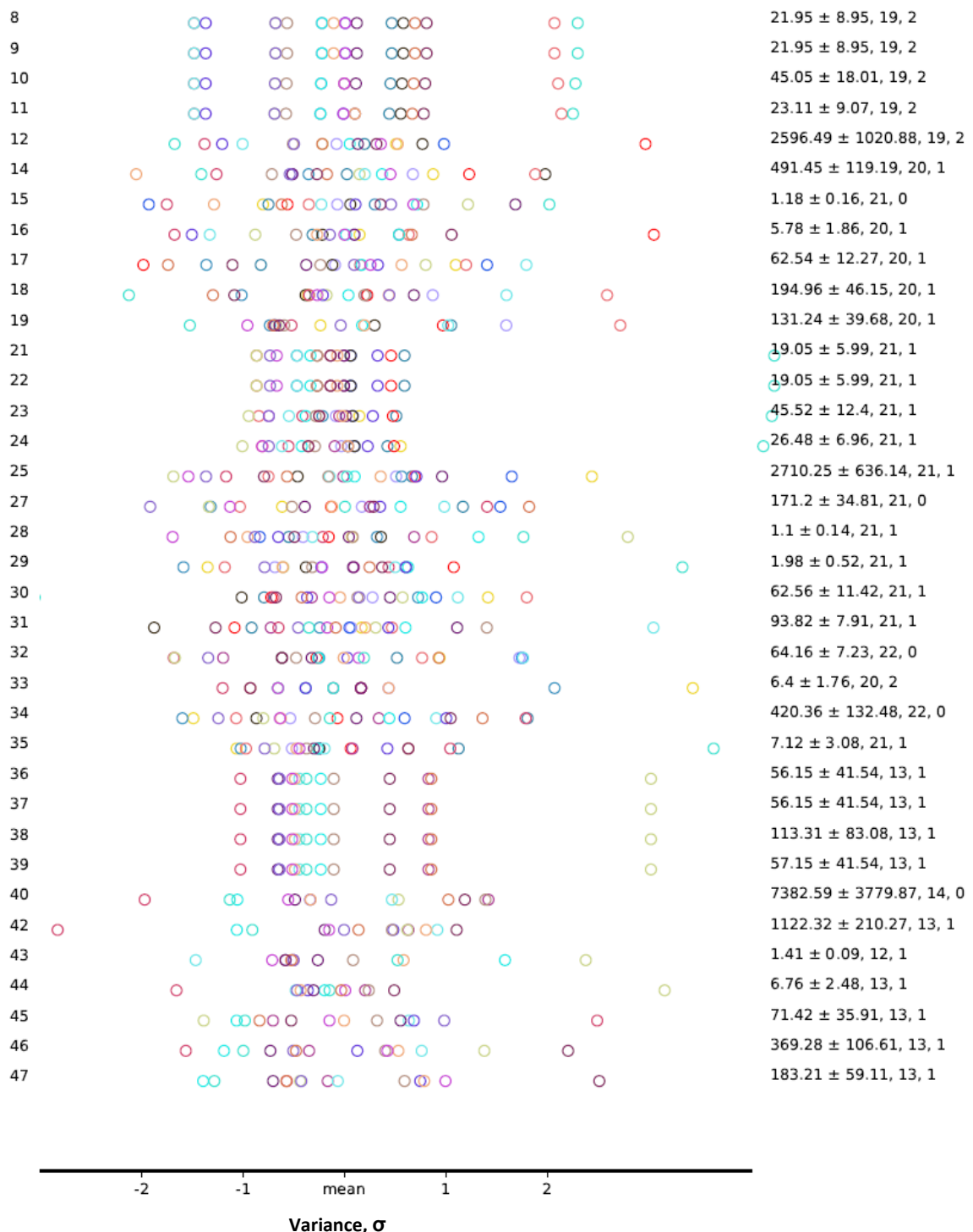


**Figure 13: Mouse L2/3 parameters distribution.**  
Parameters presentation is as described in figure 8.

## Rat L2/3

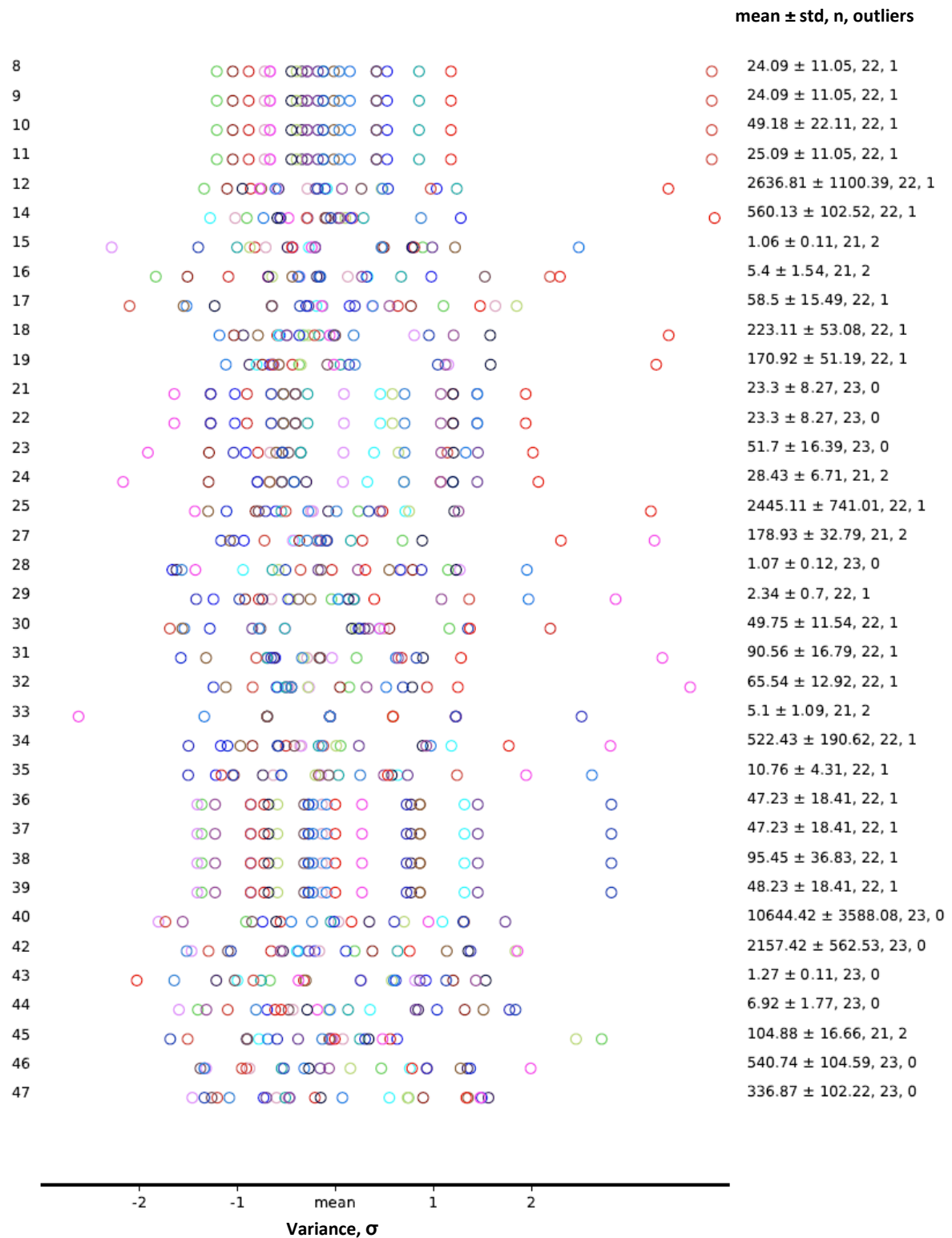


**Figure 14: Rat L2/3 parameters distribution.**

Parameter presentation is as described in figure 8.

## Human L2/3

mean  $\pm$  std, n, outliers

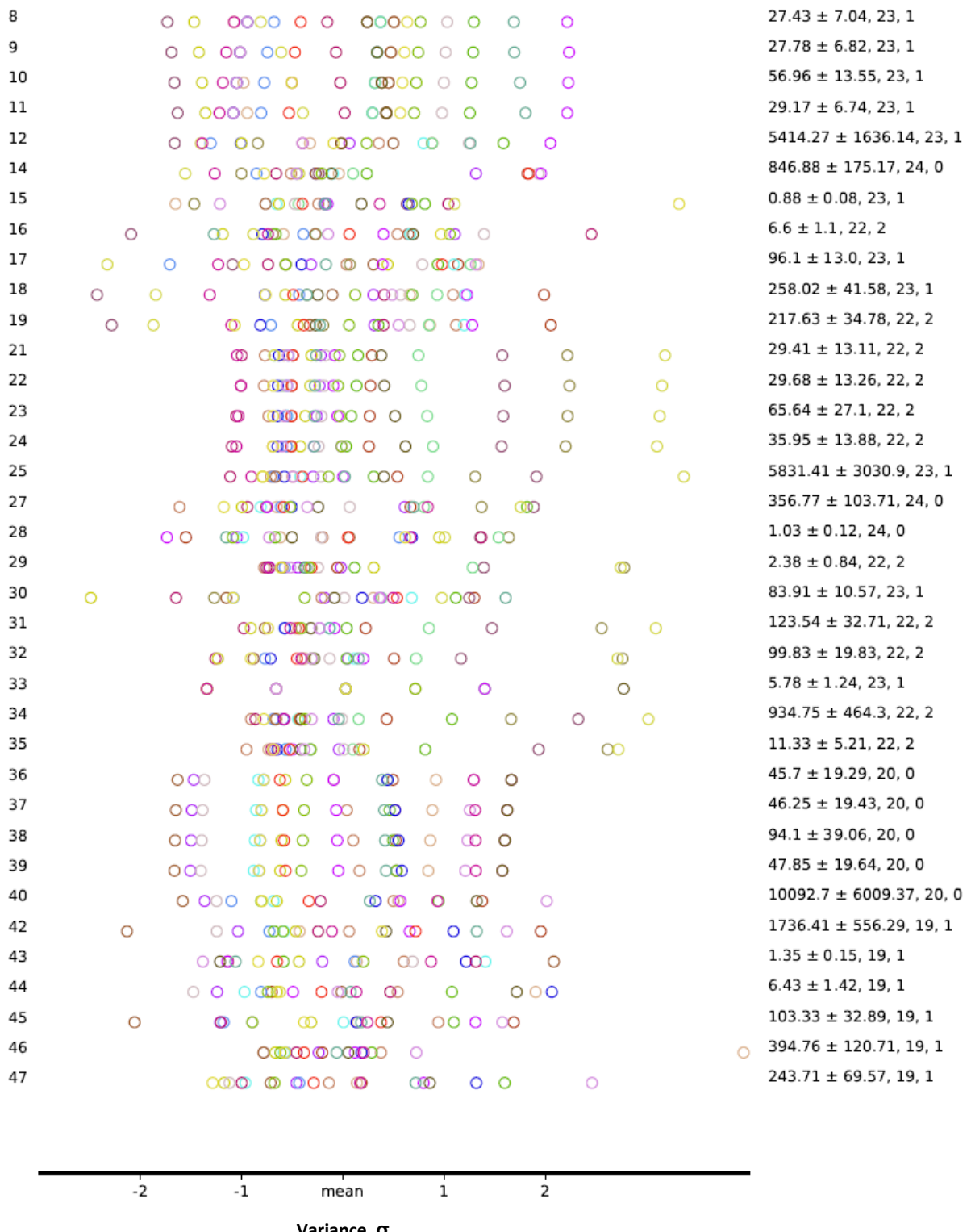


**Figure 15: Human L2/3 parameters distribution.**  
Parameters presentation is as described in figure 8.

## Rat L5

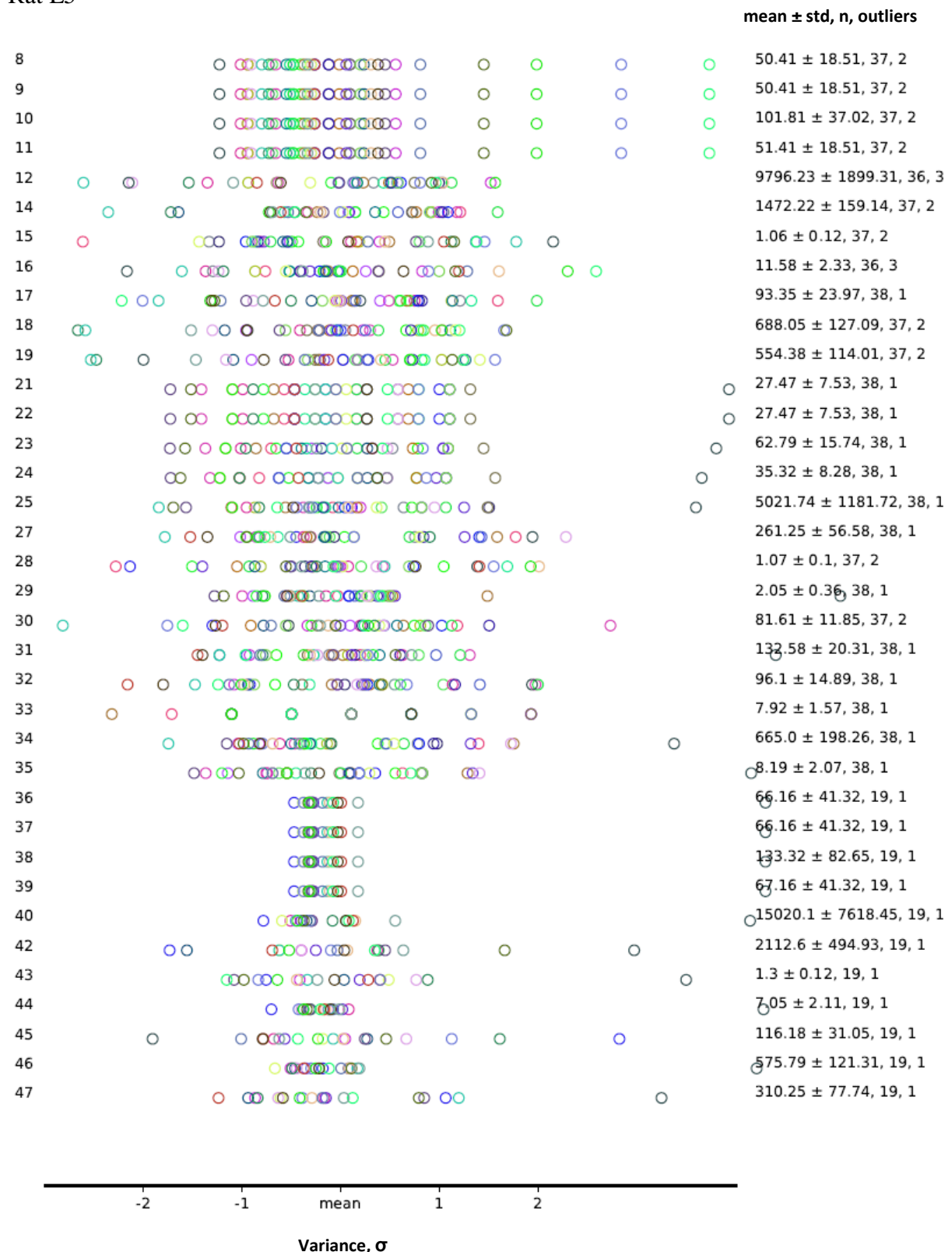


**Figure 16: Rat L5 parameters distribution.**  
Parameter presentation is as described in figure 8.

## Rat INs

**mean  $\pm$  std, n, outliers**

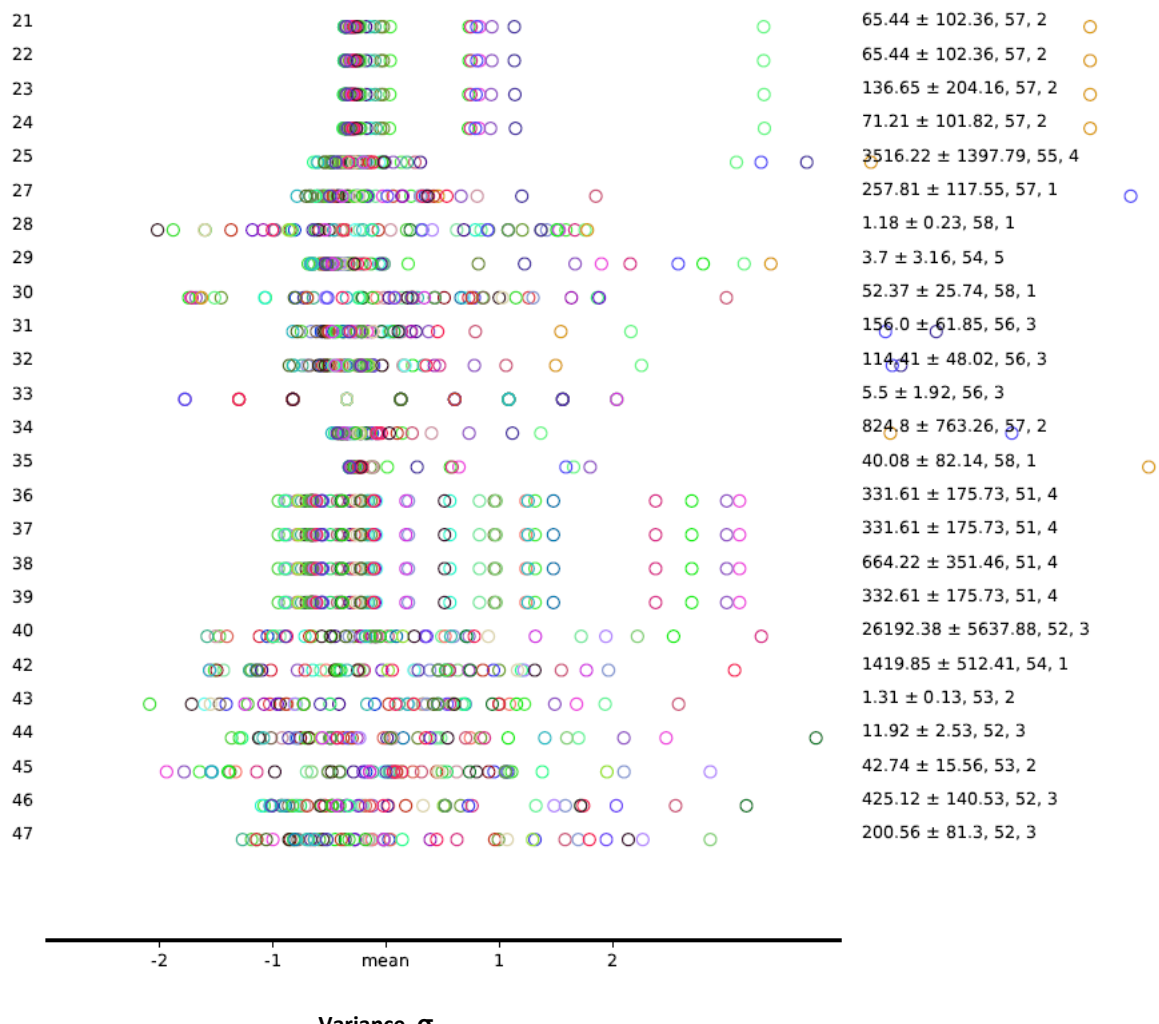


**Figure 17: Rat INs parameters distribution.**

Parameter presentation is as described in figure 8.

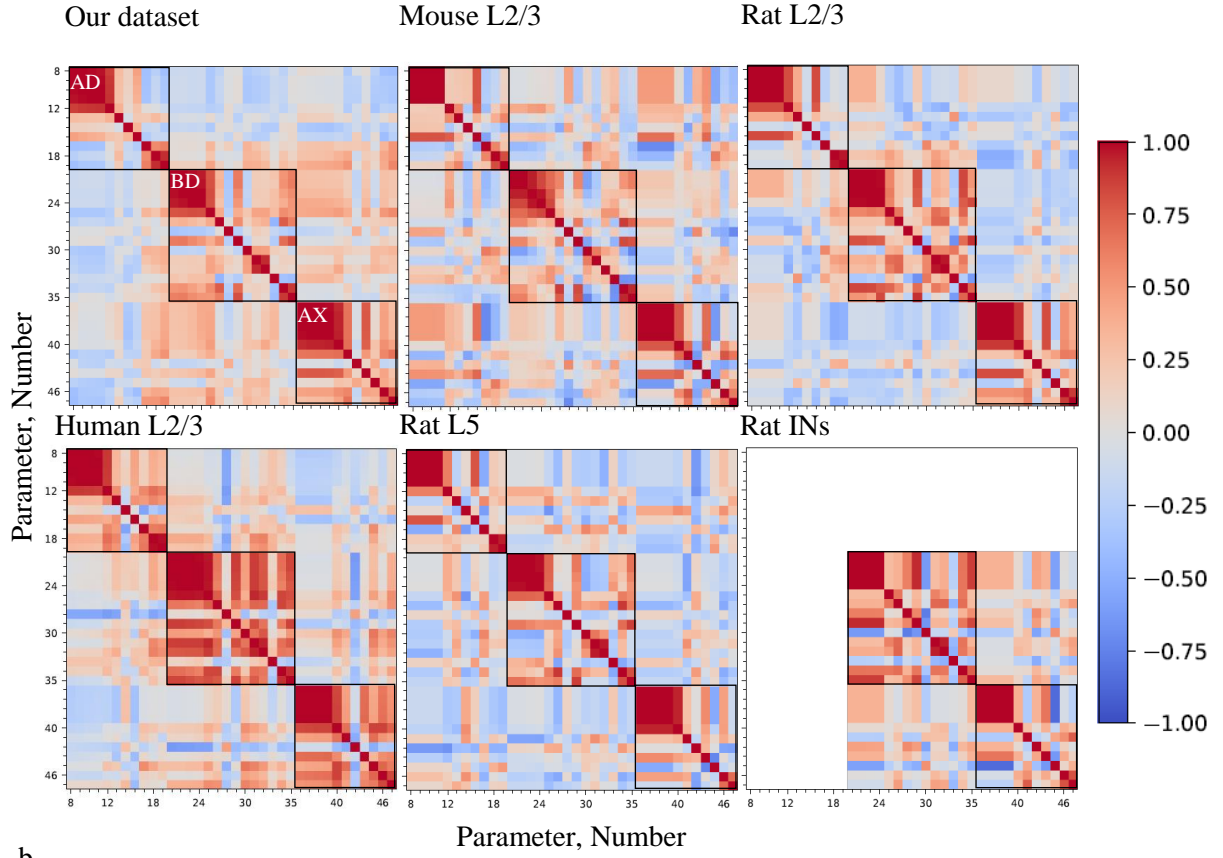
### **5.5. Meta data analysis:**

As we analyzed our dataset, we ran correlation analysis for each different dataset between all possible pairs of the parameters and preformed the same FDR statistical test (Figure 18). This parallel analysis enables us to compare the rules of relation between different anatomical parameters we found for mouse AC L2\3 PyrNs anatomy to PyrNs and INs in other species and layers of the neocortex.

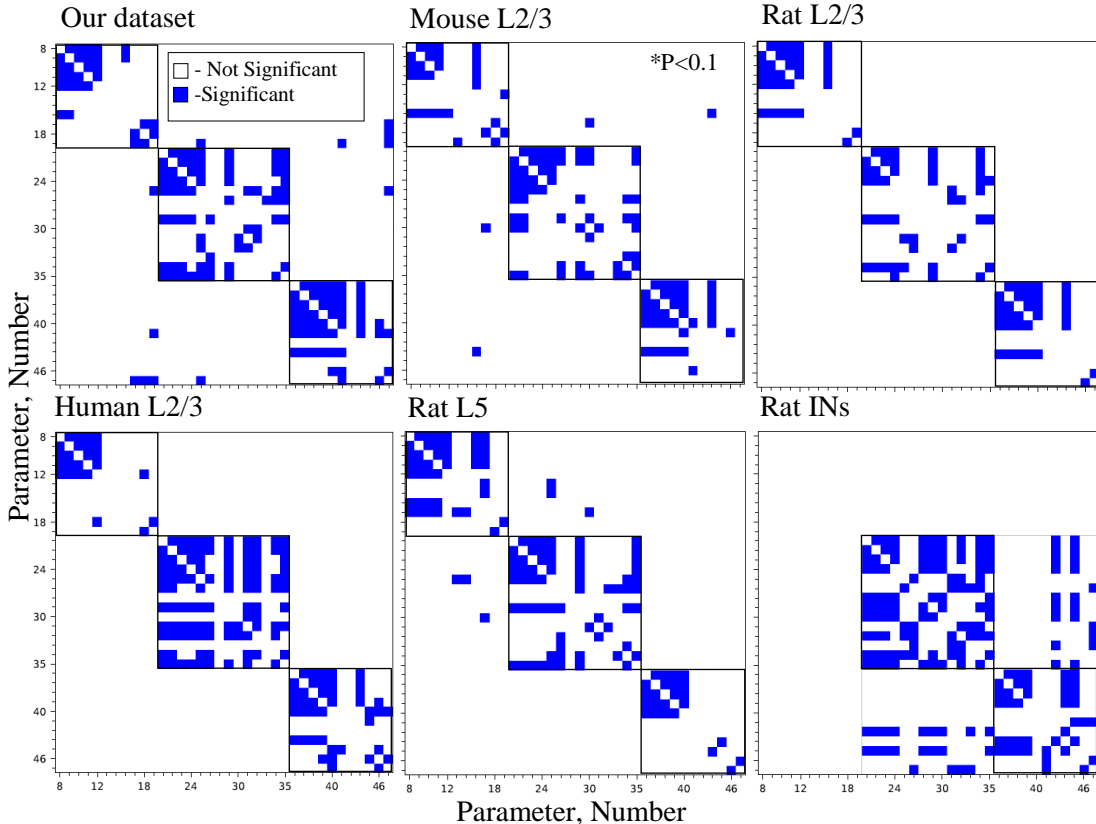
As we expected, the rat INs dataset exhibits very different significant correlations compare to our dataset and other PyrNs datasets which demonstrate more or less similar patterns of correlations (Figure 18b). However, due to poor quality (incomplete neurites trees, shrinkage, different research groups etc.) and small samples of the other datasets, they probably didn't exhibit all the correlations we found in our dataset. The more qualitative the data, the more similar its significant correlation to those of our dataset (e.g. Human L2/3 dataset, Figure 18), and hence, it is possible there may be very clear rules for the anatomy of PyrNs. In order to test it mathematically, we used our dataset to construct formulas that predict the other datasets values and examined their compatibility with their real values. Sample size and data's quality have no effect on the prediction and will not constitute a deterrent to the validity of the results.

Eventually, our research was assigned to test the possibility to predict neuroanatomy features from one L2/3 pyramidal cell to another pyramidal cell in this layer, and hopefully to be expanded to other brain areas, layers and species. In order to evaluate the ability of the significant correlations we found in our dataset to predict the values of specific parameters in other datasets, we performed 'train and test' procedure. In this test we "trained" the independent parameter in the new dataset to predict the dependent parameter in accordance with the rule (i.e. significant correlation) we found in our data. In the next step, we examined how much the prediction is close to the real values of the dependent parameter (the mean square error (MSE) value), we made a comparison between the MSE we got in our dataset to the new MSE of the other dataset by F-TEST for variance comparing. If there is a significant difference between the MSE's values, then the ability of our dataset to predict by the specific correlation wouldn't exist, however, if there is a similarity, it indicates that the prediction is acceptable. In figure 19a we showed color map with all the significant correlations we found in our dataset colored by dark grey. The color maps for the other datasets (Figure 19b-f) were colored at the same location by blue and red, which represent the significance difference/similarity of the MSE's values.

a



b

**Figure 18: Comparison of correlations color maps.**

Display of correlations and their significance for all pairs of parameters. The numbers in the axes represent the number of the parameter and the colors represent the level of the correlation or the significance. a. R values color map for each dataset. The colors represent the R values as described in figure 10. b. Q values color maps in which significant correlations ( $q < 0.01$ ) represented by blue and the non-significant by white.

We found that Rat L2/3 dataset had the highest capability for prediction since all the relevant correlations colored by red. Next were the Human L2/3 and rat L5 datasets. One would expect that mouse L2/3 dataset should be the most similar to ours, but apparently these differences stem from the low sample size of high-quality mouse L2/3 PyrNs reconstructions deposited to date. In figure 19b, MSE's correlations of parameters 21-24 are colored by blue. The explanation for the significant differences between the mouse L2/3 dataset to our dataset, although those parameters actually represent the same feature of the neuron, is due to errors in the mouse L2/3 dataset reconstructions, which can be seen by two outliers in the regression lines. In addition, the blue dots in the human L2/3 dataset on parameters 36-40 (Figure 19d), indicate that our dataset cannot predict the correlation between AX length and some of its geometrical features. This specific discrepancy is probably due to the thickness of the slice of human cortex (300  $\mu$ m) relative to PyrNs increased size in the human brain (Deitcher et al., 2017). Thus, the relative volume of cortical tissue surrounding the soma used for AX reconstructions in this dataset, is nominal and doesn't represent the AX geometrical rules.

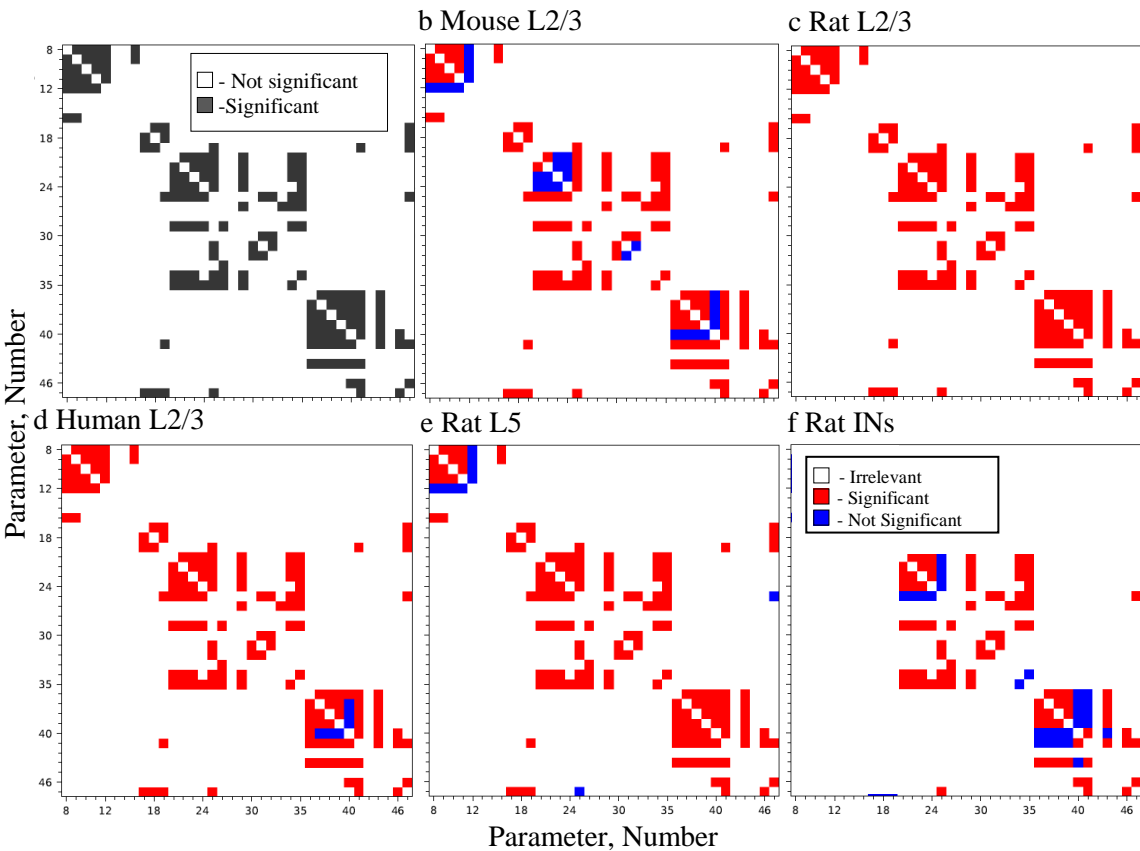


**Figure 19: MSE's significance of different datasets.**

- Our dataset significant correlations colored by dark grey.
- Displays of MSE's comparison and its significance with any significant correlation of our dataset to the same correlation in the other datasets. The numbers in the axes represent the number of the parameter. The red color represents non-significant p-value ( $p>0.01$ ), and hence similarity between the MSE's, the blue represents significant p-value and hence different MSE's values and the white is irrelevant correlations which were not significant in our dataset.

## **6. Discussion**

Our main aim in this research was to characterize L2/3 PyrNs in mouse AC. In most of the neuroanatomy studies, neuronal morphological parameters were extracted from images acquired *in vitro* and hence lacking complete reconstruction of cell neuroanatomy and do not relate to SSP. Hence, we extracted cell's neuroanatomy and SSP of L2/3 PyrNs from *in vivo* time lapse imaging followed by creation of unique dataset which enable us, for the first time, to test the relation between SSP and neuroanatomy. Moreover, this elaborated database enables us to compare the neuroanatomy of PyrNs in various mammalian species and identify geometrical rules which form a blueprint for L2/3 PyrNs neuroanatomy.

### **6.1. Structural plasticity of PyrNs**

By *in vivo* time lapse imaging we could repeatedly sample cell's neuroanatomy over time and measure the anatomical changes in synaptic and neurites structures. We found that structure of PyrNs neurites over time remains stable and hardly changes (Figure 6). The minor changes that were observed were addition or elimination of short terminal branches (5-30  $\mu\text{m}$ ). However, these changes were identified in a small fraction of cell sampled (2/15, Figure 6). This result is consistent with studies which suggest that apart from their dendritic spines, dendritic arbors of pyramidal neurons are largely stable in the adult cortex (Chen & Nedivi, 2010; Lee et al., 2006; Trachtenberg et al., 2002). Also, they found that in the neocortex of primates, horizontally projecting AXs of L2/3 PyrNs boutons have a turnover rate of 7-12% per week under normal conditions (comparable to the 13.9% per 9 days we have reported, figure 5) but whose arbors appear stable (Chen & Nedivi, 2010). Similarly, we could not identify significant changes in L2/3 PyrNs neuroanatomy over time, while we could easily monitor changes in synaptic structures on stable neurites sections (Figure 3k).

Since we monitor the morphology of synaptic structure on identified neurites sections, we were able to look for correlations between density and turnover rates to section location within L1-3. We found that SSP exhibits diverse patterns on different neurites types (AD, BD and AX) of the same cell (Figure 5). This observation was later extended to all cells in our data base. As been previously shown (De Paola et al., 2006), dendritic spines are denser than axonal boutons, however, we found that their turnover rate is much higher for apical spines than basal spines (Figure 5). Also, we found that for ADs, there is a strong negative correlation between turnover rates to section sub-pial depth (Figure 7c). In addition, we found negative correlation between BD spines turnover and section sub-pial depth (Table 1). Thus, it seems there are different connectivity pattern and computational functions for AD and BD

probably due to different inputs composition (Brown, Gillette, & Ascoli, 2008; Spurston, 2008). Indeed, several studies suggest that there is different amount of thalamic input from L4 to L2/3 that depends on the cell position in the lamina. Neurons located higher in L2/3 receive less L4 input compared to the deeper neurons which receive most of L4 input to L2/3 (Meng, Winkowski, Kao & Kanold, 2017; Meyer et al., 2010; Oberlaender et al., 2011). In addition, Spurston suggested that the basal and proximal ADs of L2/3 PyrNs receive inputs from L4 cells and also receive local-circuit excitation. The apical tuft of L2/3 PyrNs receives inputs from other cortical areas and also receives nonspecific thalamic inputs (Spurston, 2008). Thus, it seems that BD spines receiving homogenous thalamic inputs are much less plastic relative to AD spines which receive heterogeneous inputs from other cortical areas.

Moreover, spine density of AD and BD is higher when the soma is located closer to the pia surface, and they are also positively correlated to each other (Figures 7 and 11d). This result is in agreement with previous publication reporting that in contrast to L3 neurons, L2 neurons have a small size and show low excitability (Aerde & Feldmeyer, 2013). This low excitability of PyrNs, located closer to the pia surface, due to heterogeneous inputs from other cortical areas could be compensated by rise of spine density thus driving action potentials generation under this heterogeneous inputs' regime.

## **6.2. *Mouse L2/3 PyrNs anatomical blueprint***

Since our dataset enables detailed description of PyrNs complete and undistorted neuroanatomy as well as description of synaptic structure density and turnover rate for identified neurons, we could for the first time correlate between a cell neurites anatomy and SSP.

Based on neuroanatomy, generally, AC L2/3 PyrNs are homogeneous population. As we found (Figure 8), there is moderate variance in morphological parameters and the standard deviation of all parameters is substantially smaller than their mean. This is compatible with the study of Granato et al. and Oberlander et al. (Granato & De Giorgio, 2014; Oberlaender et al., 2011). However, electrical recordings studies have suggested that there are sub groups of L3 PyrNs that differ in their electrophysiological properties (Aerde & Feldmeyer, 2013).

We found positive correlations between soma depth and section radial distance of AD and AX which are also correlated positively with each other (Figures 10, 11). We assume that deeper in L2/3, the section radial distance of the AD tends to be longer as it ascends toward L1. The study of Aerde et al. suggested that a prominent feature of L2 PyrNs is their very

short apical trunk (Aerde & Feldmeyer, 2013). However, what about the AX? Studies have shown that in contrast to L2 pyramidal cells, L3 pyramidal cells have more complex dendritic arbors (Ojima, Honda & Jones, 1991; Winer, 1984), and are the source as well as the target of the majority of local, ipsilateral, and contralateral cortical, as well as thalamic connections (Code & Winer, 1985; Winguth & Winer, 1986). Hence, deeper neurons in L2/3 might have longer AXs sections in order to send output to distant areas. In addition, we found that total length of BDs positively correlates with section radial distance of AD (Figures 10 and 11). This is also compatible with those studies, when section radial distance is longer, the neuron position is deeper, and it has more complex dendritic arbors. These alterations in cell's neuroanatomy could also be manifested as altered electrophysiological properties as was previously reported (Aerde & Feldmeyer, 2013).

Independently, we found higher probability for cells with oblique AD in upper L2/3 (Figure 11l). We found that PyrNs with oblique AD constitute a significant portion of upper L2/3 neurons. Indeed, Oberlaender et al. suggested in their study that L2 PyrNs populating upper L2/3 and display short oblique ADs that spread beyond the tangential column border. In comparison, the L3 PyrNs were located in deeper supragranular regions and exhibited ADs that projected mostly parallel to the vertical column axis and ended with narrow tufts in L1 (Oberlaender et al., 2011). However, another study found that the angle of the main AD to the columnar axis was not correlated with the distance of the soma from the pia surface (Hardingham et al., 2011). In order to clarify this issue, further study relating to the encoding function of cells with oblique AD in upper L2/3, is required.

For the first time, we could investigate the relationship between PyrNs neuroanatomy and its SSP. We found that the sum length of the neuron's neurites and number of bifurcations of AX positively correlate with apical turnover rate (Figure 11j, k). Thus, it seems that the more complex the neuron's neurites, there is a higher probability for SSP on its AD. We could not identify any references in the literature that could explain these findings. We assume that complex cells have higher turnover rates and seems to have a higher probability to impact learning and memory in L2/3, and their bigger and more complex AXs suggest they could act as a hub controlling and driving rewiring of the cortical circuit. Similarly, we found that total length of BDs is positively correlated with number of boutons. Moreover, there is a strong relation between total length of BD to the total length of an AX ( $r = 0.48$ ,  $q = 0.0153$ ). The interaction between AX boutons density and AX length (e.g. total number of boutons) increases the significance to the correlation with BD length. Thus, bigger dendrites will go together with bigger AX and higher SSP.

### **6.3. L2/3 PyrNs anatomical blueprint conservation**

The neocortex is the newest part of the cerebral cortex to evolve and is involved in higher-order brain functions (Lodato & Arlotta, 2015). Thus, it appears to be a distinguishing feature of mammals; it has been found in the brains of all mammals, but not in those of any other animals (Rakic, 2009). One of the aims of our study is to see if PyrNs anatomical blueprint is conserved between species. The quality of the other datasets of PyrNs neuroanatomy we used (Figures 12-17) is not the same as ours, thus we probably cannot reliably extract all the correlations we identify in our dataset. Nevertheless, in general, we could conclude that L2/3 PyrNs anatomical blueprint is conserved between mouse, rat and humans (Figure 19a, c and d). It is known that *in vitro* reconstruction has its limitations. The study of Jaap et al. shows that in 300  $\mu\text{m}$  thick slices, intracortical AXs lost about 50% and dendrites about 16% of their mass (Jaap, Arjen & Harry, 2014). Costa et al. used data from neuromorpho to examine the neurons net, and performed PCA on the morphology (Costa, Zawadzki, Miazaki, Viana & Taraskin, 2010). Their findings and their conclusions are not reliable considering the partial information in these datasets. Another research compared between three similar datasets (some data was taken *in vitro* and some *in vivo*), but from three different research groups, and found significant morphometric difference between the measurements (Szilagyi & Schutter, 2004).

We found that in our dataset the total dendritic length was significantly higher (by 41% and 47% respectively) than that of L2/3 mouse and rat reconstructions extracted from neuromorpho datasets (Figures 12-14). Also, other studies exhibit the same values for total dendritic length as neuromorpho dataset (5317  $\mu\text{m}$  in mouse (Mohan et al., 2015), 5549  $\mu\text{m}$  in rat (Aerde & Feldmeyer, 2013)). Hence, *in vivo* reconstruction reflects more reliably the morphology in PyrNs and future research in this field should take this into account. In rat L5 dataset the size and complexity of the AX and the AD is higher than our dataset, indicating that the L2/3 PyrNs anatomical blueprint is layer dependent and might be also different in other brain structures as described, for example, in Elston study that claims that PyrNs in the rat prefrontal cortex have, on average, up to 23 times more dendritic spines than those in the visual cortex (Elston, 2003). As expected, rat INs dataset differ the most in terms of the significant correlations we found indicating that the L2/3 PyrNs anatomical blueprint could not be extended to other cell types. Using MSE analysis, we could fully predict rat L2/3 correlation between pair of anatomical parameters (Figure 19). Similar results were obtained for the human and mouse L2/3 datasets. This result indicates that the anatomical blueprint of PyrNs from the same lamina is conserved between mouse, rat and humans. However, the study

of Steger et al. found that similar cell types in the rat and mouse may not always share similar physiological and morphological properties, although they did not look for correlation similarity (Steger et al., 2013). In addition, Deitcher et al. compared between human and mouse L2/3 PyrNs (Deitcher et al., 2017). In this publication the authors claimed that mouse L2/3 PyrNs from the temporal neocortex ( $n=14$ ) do not show a significant gradual change with depth and that most of their morphological features are comparable to that of human L2/3 PyrNs. This study also examined whether human derived L2/3 PyrNs were morphologically just a "scaled" version of mouse neurons; this does not seem to be the case (Deitcher et al., 2017). Our results indicate that the only feature of human L2/3 PyrNs that was "scaled" is section length indicating that the overall geometrical structure remain the same (Figures 12 and 15). In addition, Mohan et al. found that based on total dendritic length, 88% of human L2/3 neurons were classified into human-specific clusters and only 12% of human L2/3 neurons were comparable with neurons from mouse. This observation indicates that L2/3 pyramidal neurons in human temporal cortex have a distinct dendritic architecture compared with mouse. (Mohan et al., 2015)

Our results obtained from the mouse AC indicate that L2/3 PyrNs neuroanatomy exhibits variety of correlations with soma depth. Thus, we cannot rule out that there is a variance in L2/3 PyrNs composition in different cortical regions. However, since we compared data obtained in the mouse AC with data obtained in rat and human primary cortices it is plausible that the common blueprint we have identified is restricted to primary region which have similar connectivity and input and output scheme. Thus, as more reconstructions of PyrNs will become available, we should revisit our analysis scheme and expand it to identify and characterize variations from the "common" blueprint we have established for L2/3 PyrNs and try to define species and region specific variation related to PyrNs neuroanatomy.

## References

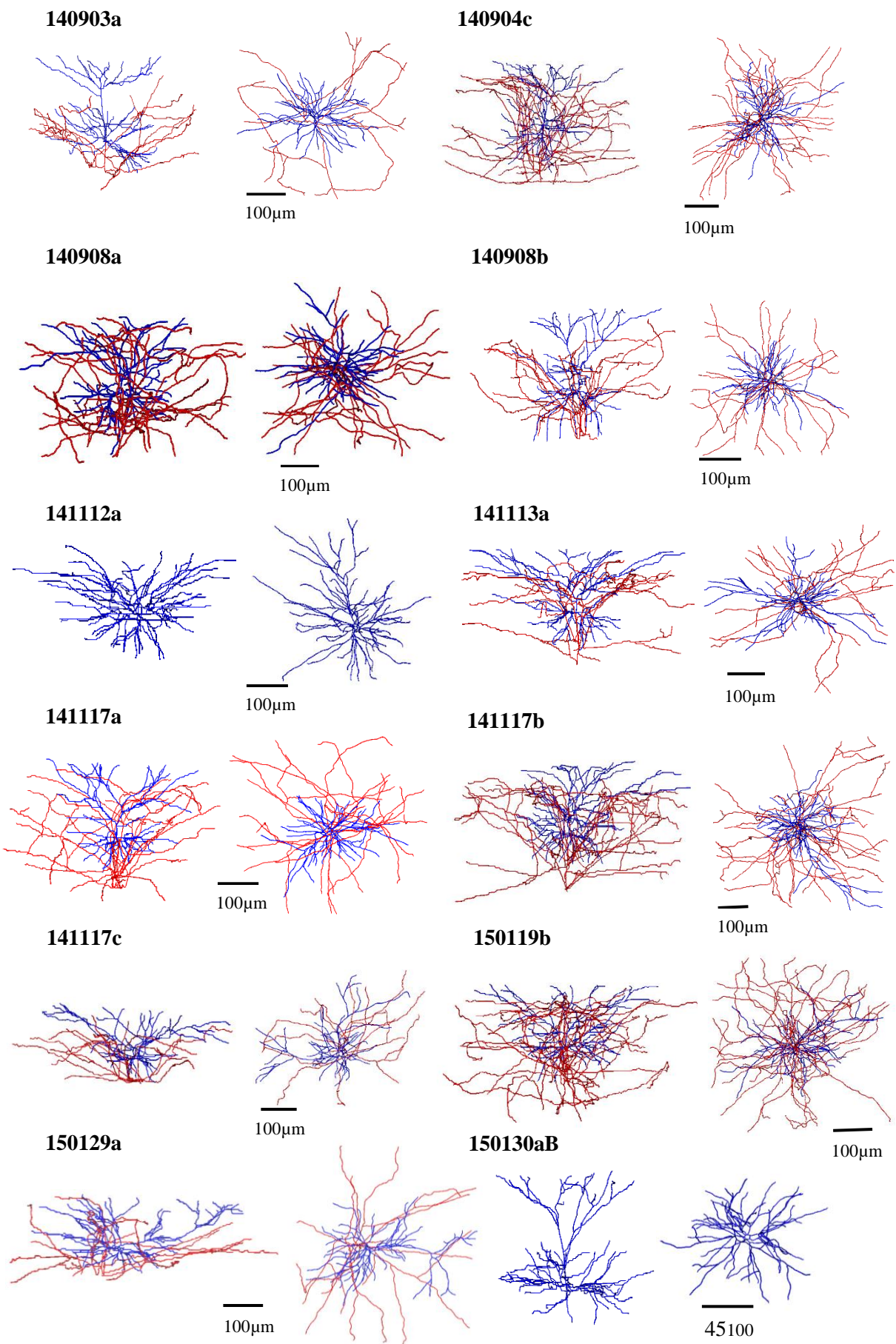
- Aerde, K. I., & Feldmeyer, D. (2013). Morphological and physiological characterization of pyramidal neuron subtypes in rat medial prefrontal cortex. *Cerebral Cortex*, 25(3), 788-805.
- Ascoli, G. A. (2006). Mobilizing the base of neuroscience data: The case of neuronal morphologies. *Nature Rev. Neurosci*, 7, 318-324.
- Bannister, A. P. (2005). Inter- and intra-laminar connections of pyramidal cells in the neocortex. *Neuroscience Research*, 53, 95-103.
- Brown, K., Gillette, T., & Ascoli, G. (2008). Quantifying neuronal size: Summing up trees and splitting the branch difference. *Seminars in Cell & Developmental Biology*, 19(6), 485-493.
- Chen, J. L., & Nedivi, E. (2010). Neuronal structural remodeling: Is it all about access? *Current Opinion in Neurobiology*, 20(5), 557-562.
- Chklovskii, D. B., Mel, B. W., & Svoboda, K. (2004). Cortical rewiring and information storage. *Nature*, 431(7010), 782-788.
- Code, R. A., & Winer, J. A. (1985). Commissural neurons in layer III of cat primary auditory cortex (AI): Pyramidal and non-pyramidal cell input. *J Comp Neurol*, 242, 485–510.
- Costa, L. D., Zawadzki, K., Miazaki, M., Viana, M. P., & Taraskin, S. N. (2010). Unveiling the neuromorphological space. *Frontiers in Computational Neuroscience*, 4.
- De Paola, V., Holtmaat, A., Knott, G., Song, S., Wilbrecht, L., Caroni, P., & Svoboda, K. (2006). Cell type-specific structural plasticity of axonal branches and boutons in the adult neocortex. *Neuron*, 49(6), 861-875.
- Deitcher, Y., Eyal, G., Kanari, L., Verhoog, M. B., Kahou, G. A., Mansvelder, H. D., . . . Segev, I. (2017). Comprehensive morpho-electrotonic analysis shows 2 distinct classes of L2 and L3 pyramidal neurons in human temporal cortex. *Cerebral Cortex*, 27(11), 5398-5414.
- Elston, G. N. (2003). Cortex, cognition and the cell: New insights into the pyramidal neuron and prefrontal function. *Cereb Cortex*, 13, 1124-1138.
- Gabbott, P. L., Warner, T. A., Jays, P. R., Salway, P., & Busby, S. J. (2005). Prefrontal cortex in the rat: Projections to subcortical autonomic, motor, and limbic centers. *J Comp Neurol*, 492, 145-177.
- Granato, A., De Giorgio, A. (2014). Alterations of neocortical pyramidal neurons: Turning points in the genesis of mental retardation. *Frontiers In Pediatrics*, 2, 86.
- Hardingham, N. R., Gould, T., & Fox, K. (2011). Anatomical and sensory experiential determinants of synaptic plasticity in layer 2/3 pyramidal neurons of mouse barrel cortex. *The Journal of Comparative Neurology*, 519, 2090-2124.

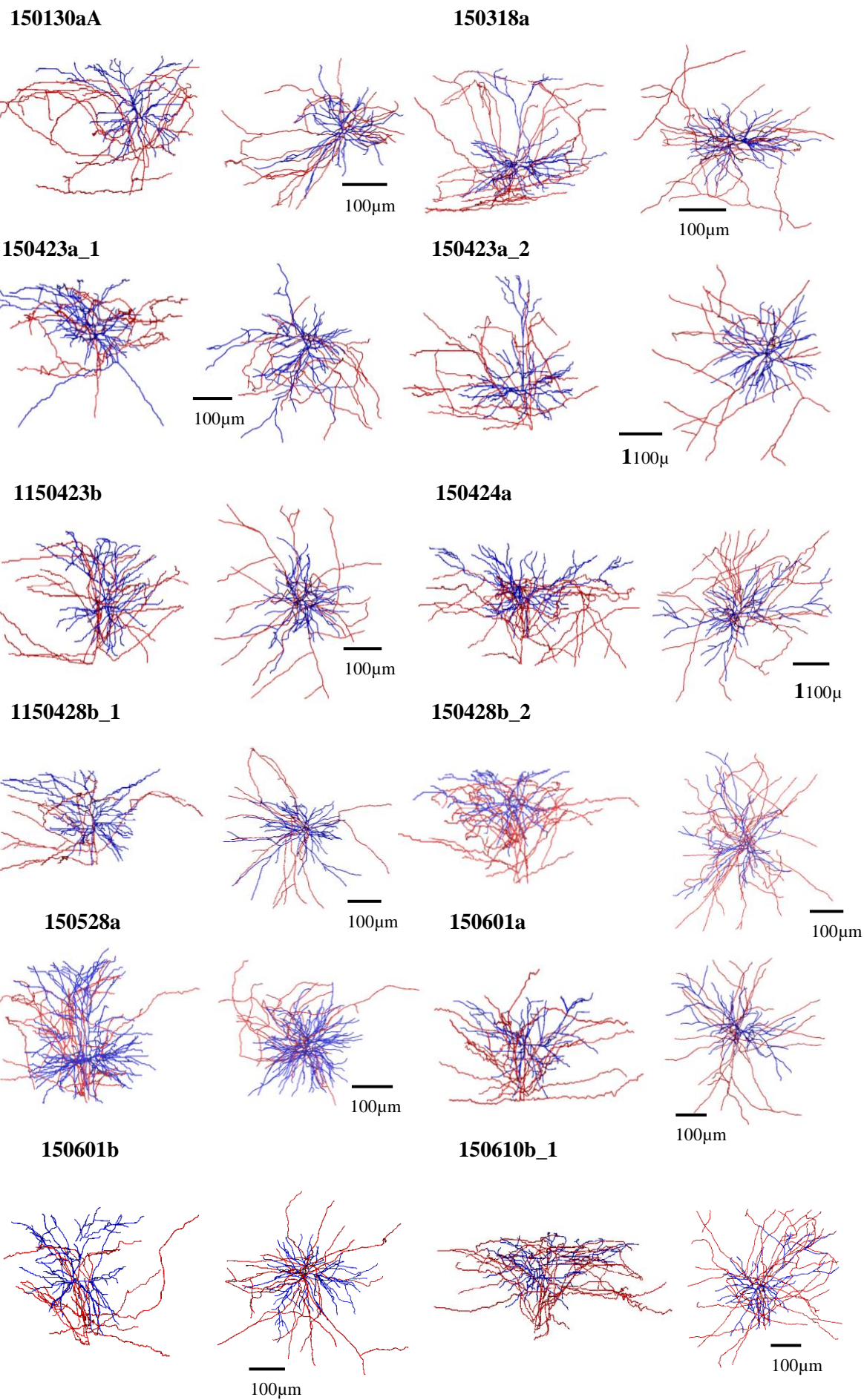
- Helbling, S., Teki, S., Callaghan, M. F., Sedley, W., Mohammadi, S., Griffiths, T. D., Weiskopf, N., & Barnes, G.R. (2015). Structure predicts function: Combining non-invasive electrophysiology with in-vivo histology. *NeuroImage*, 108, 377-385.
- Jaap, V. P., Arjen, V. O., & Harry, U. (2014). Axonal and dendritic density field estimation from incomplete single-slice neuronal reconstructions. *Frontiers in Neuroinformatics*, 8.
- Holtmaat, A. J., Trachtenberg, J. T., Wilbrecht, L., Shepherd, G. M., Zhang, X., Knott, G. W., & Svoboda, K. (2005). Transient and persistent dendritic spines in the neocortex in vivo. *Neuron*, 45(2), 279-291.
- Lee, W.C., Huang, H., Feng, G., Sanes, J.R., Brown, E.N., So, P. T., & Nedivi, E. (2006). Dynamic remodeling of dendritic arbors in GABAergic interneurons of adult visual cortex. *PLoS Biol*, 4(29).
- Lodato, S., & Arlotta, P. (2015). Generating neuronal diversity in the mammalian cerebral cortex. *Annual Review of Cell and Developmental Biology*, 31, 699–720.
- Mason, A., & Larkman, A. (1990). Correlations between morphology and electrophysiology of pyramidal neurons in slices of rat visual cortex. *The Journal of Neuroscience: The Official Journal of the Society for Neuroscience*, 10, 1415-1428.
- Megías, M., Emri, Z., Freund, T. F., & Gulyás, A. I. (2001). Total number and distribution of inhibitory and excitatory synapses on hippocampal CA1 pyramidal cells. *Neuroscience* 102(3), 527–540.
- Meng, X., Winkowski, D. E., Kao, J. P., & Kanold, P. O. (2017). Sublaminar subdivision of mouse auditory cortex layer 2/3 based on functional translaminar connections. *The Journal of Neuroscience*, 37(42), 10200-10214.
- Meyer, H. S., Wimmer, V. C., Hemberger, M., Bruno, R. M., Kock, C. P., Frick, A., . . . Helmstaedter, M. (2010). Cell type-specific thalamic innervation in a column of rat vibrissal cortex. *Cerebral Cortex*, 20(10), 2287-2303.
- Mohan, H., Verhoog, M. B., Doreswamy, K. K., Eyal, G., Aardse, R., Lodder, B. N., Goriounova, N. A., Asamoah, B., Brakspear, A. B., Groot, C., et al. (2015). Dendritic and axonal architecture of individual pyramidal neurons across layers of adult human neocortex. *Cereb Cortex*, 25, 4839–4853.
- Moore, C. I., Carlen, M., Knoblich, U., & Cardin, J. A. (2010). Neocortical interneurons: From diversity, strength. *Cell*, 142, 189–93.
- Narayanan, R. T., Egger, R., Johnson, A. S., Mansvelder, H. D., Sakmann, B., de Kock, C. P. J., & Oberlaender, M. (2015). Beyond columnar organization: Cell type- and target layer-specific principles of horizontal axon projection patterns in rat vibrissal cortex. *Cerebral Cortex*, 25(11), 4450–4468.

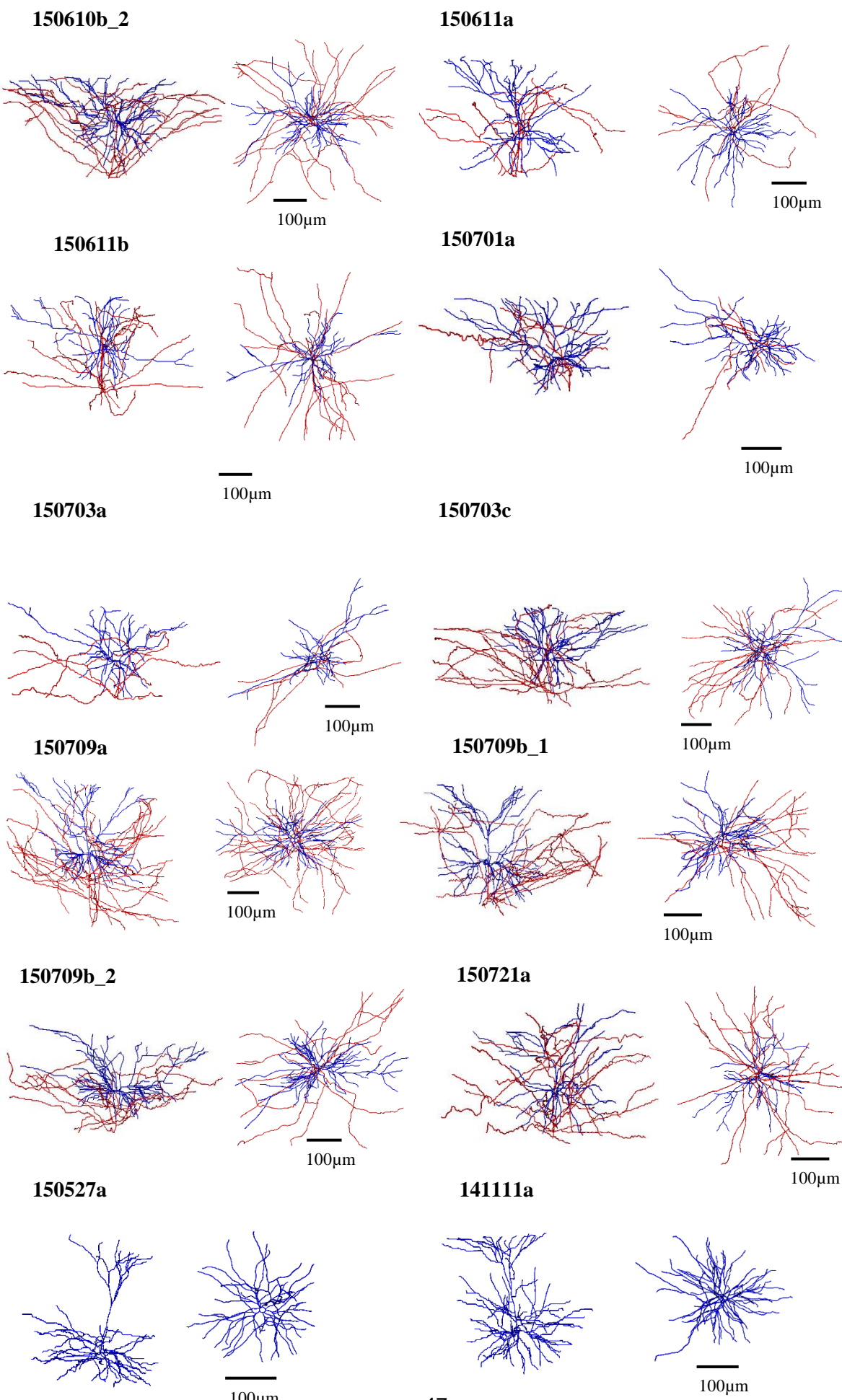
- Noback, C. R. (2005). The human nervous system: Structure and function. *Totowa, NJ: Humana Press.*
- Oberlaender, M., De Kock, C. P., Bruno, R. M., Ramirez, A., Meyer, H. S., Dercksen, V. J., Helmstaedter, M., & Sakmann, B. (2011). Cell type-specific three-dimensional structure of thalamocortical circuits in a column of rat vibrissal cortex. *Cereb Cortex*, 22, 2375-2391.
- Ojima, H., Honda, C. N., & Jones, E. G. (1991). Patterns of axon collateralization of identified supragranular pyramidal neurons in the cat auditory cortex. *Cereb Cortex*, 1, 80–94.
- Petersen, C. C., & Crochet, S. (2013). Synaptic computation and sensory processing in neocortical layer 2/3. *Neuron*, 78, 28-48.
- Ramón y Cajal, S. (1995). Histology of the nervous system of man and vertebrates. *New York: Oxford University Press.*
- Rakic, P. (2009). Evolution of the neocortex: Perspective from developmental biology. *Nature Reviews Neuroscience*, 10(10), 724–735.
- Rodney, J., & Kevan, A. C. (2004). Neuronal circuits of the neocortex. *Annual Reviews Neuroscience*, 27, 419-451.
- Sadakane, O., Masamizu, Y., Watakabe, A., Terada, S., Ohtsuka, M., Takaji, M., . . . Yamamori, T. (2015). Long-term two-photon calcium imaging of neuronal populations with subcellular resolution in adult non-human primates. *Cell Reports*, 13(9), 1989-1999.
- Spruston, N. (2008). Pyramidal neurons: Dendritic structure and synaptic integration. *Nature Reviews Neuroscience*, 9, 206-221.
- Steger, R. M., Ramos, R. L., Cao, R., Yang, Q., Chen, C. C., Dominici, J., & Brumberg, J. C. (2013). Physiology and morphology of inverted pyramidal neurons in the rodent neocortex. *Neuroscience*, 248, 165-179.
- Szilagyi, T., & Schutter, E. D. (2004). Effects of variability in anatomical reconstruction techniques on models of synaptic integration by dendrites: A comparison of three internet archives. *European Journal of Neuroscience*, 19(5), 1257-1266.
- Trachtenberg, J. T., Chen, B. E., Knott, G. W., Feng, G., Sanes, J. R., Welker, E., & Svoboda, K. (2002). Long-term in vivo imaging of experience-dependent synaptic plasticity in adult cortex. *Nature*, 420, 788–794.
- Ueta, Y., Otsuka, T., Morishima, M., Ushimaru, M., & Kawaguchi, Y. (2014). Multiple layer 5 pyramidal cell subtypes relay cortical feedback from secondary to primary motor areas in rats. *Cereb Cortex*, 24, 2362-2376.
- Watson, C., & Paxinos, G. (2010). Chemoarchitectonic atlas of the mouse brain. *First ed. San Diego: Academic Press.*

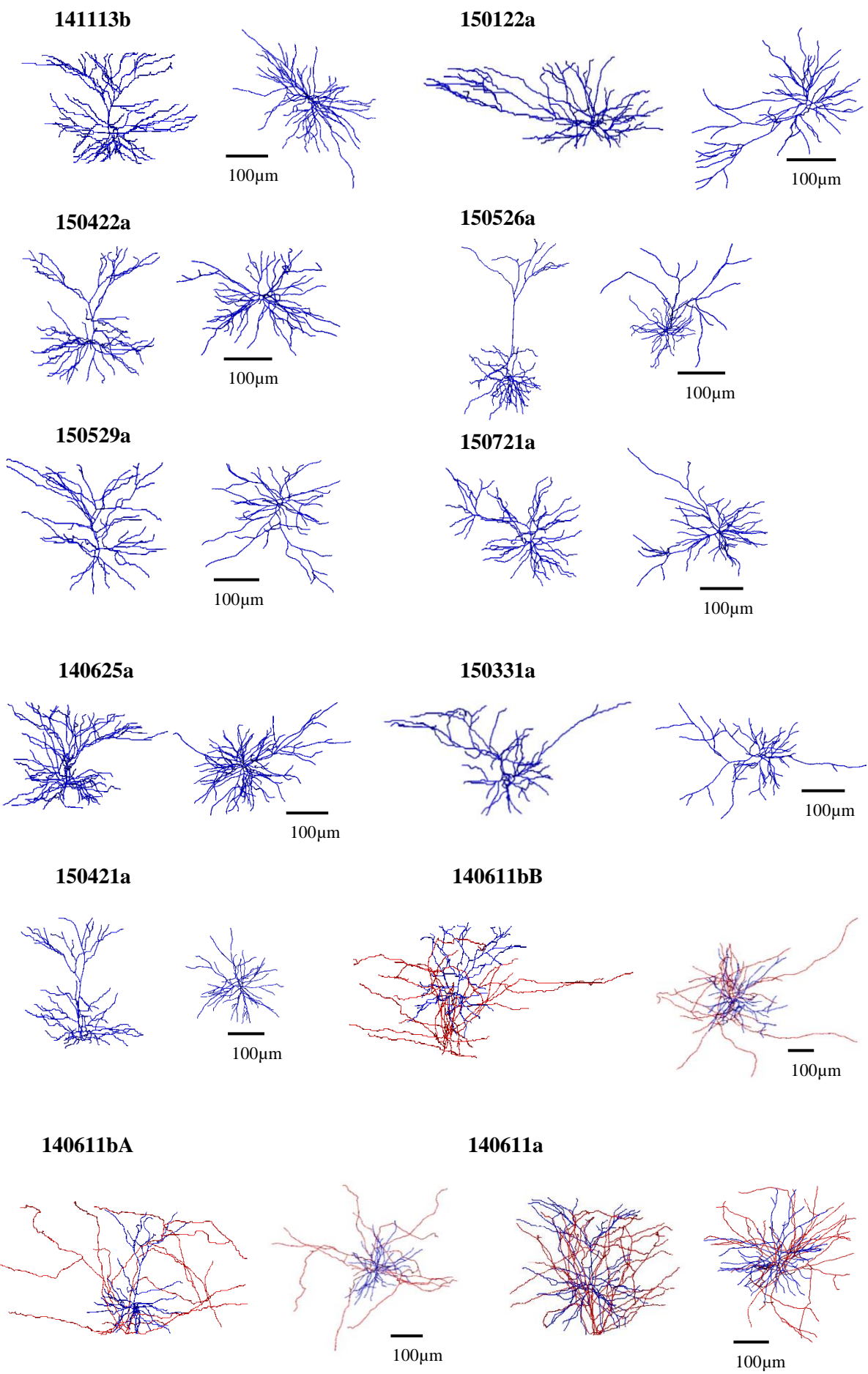
- Winer, J. A. (1984). The pyramidal neurons in layer III of cat primary auditory cortex (AI). *J Comp Neurol*, 229, 476–496.
- Winguth, S. D., Winer, J. A. (1986). Corticocortical connections of cat primary auditory cortex (AI): Laminar organization and identification of supragranular neurons projection to area AII. *J Comp Neurol*, 248, 36 –56.

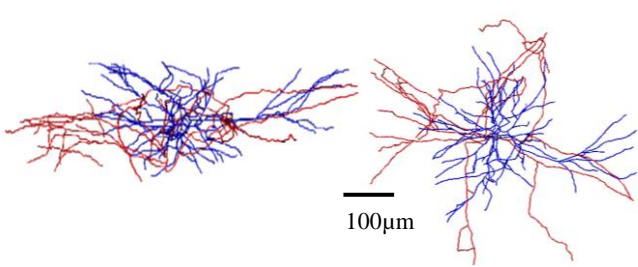
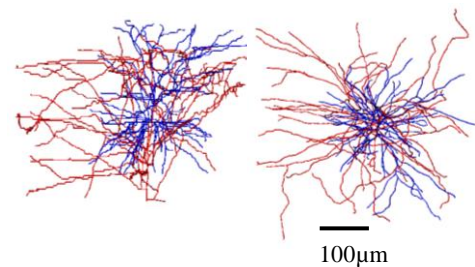
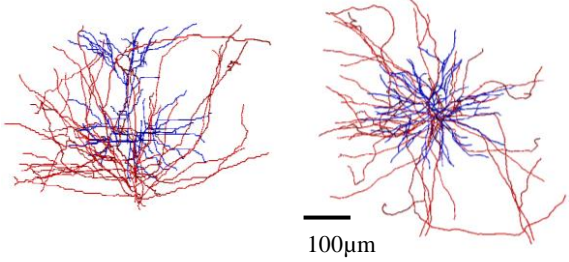
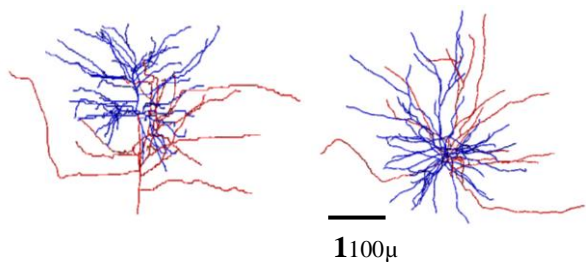
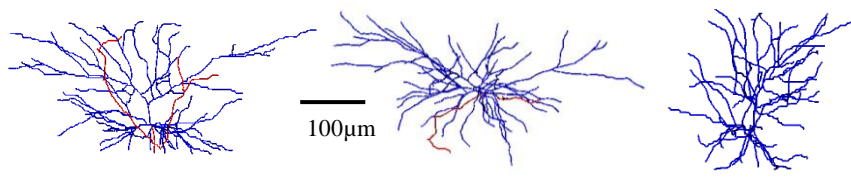
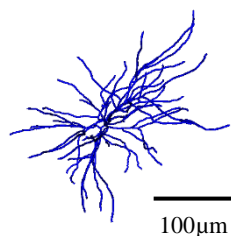
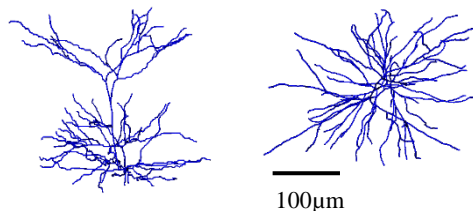
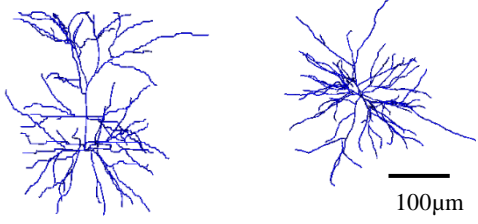
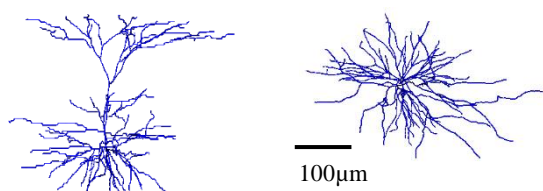
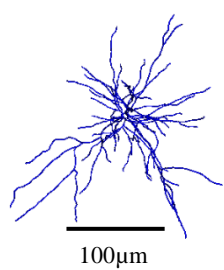
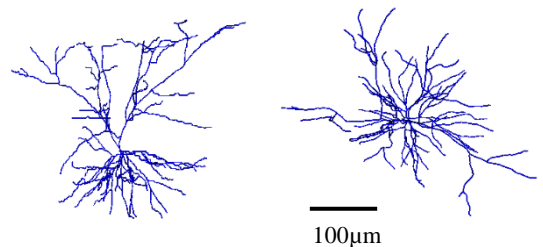
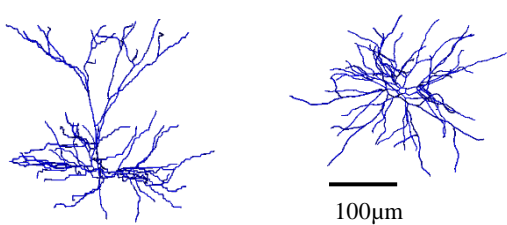
## Appendix 1: Layer 2/3 PyrNs reconstruction.



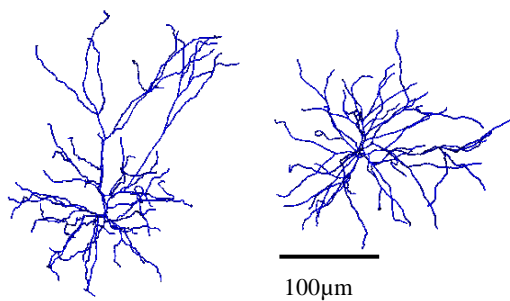




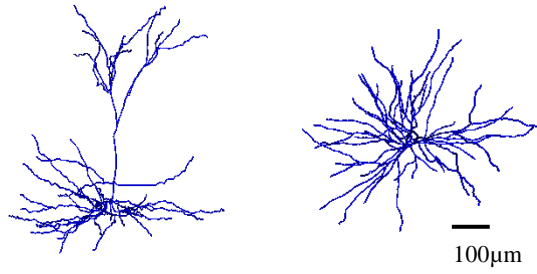


**140909a****141118a****1141118c****1150119a****1150422b****140625b****140630b****1400909a\_1A****1400909a\_1B****140909bA****140909bB****150130aA**

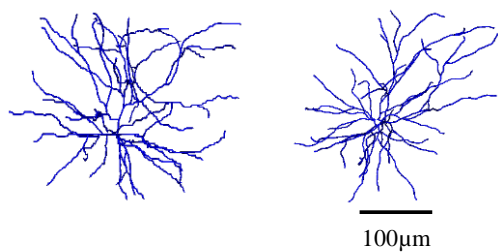
**150610aA**



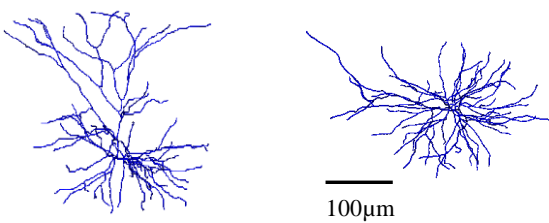
**150610aB**



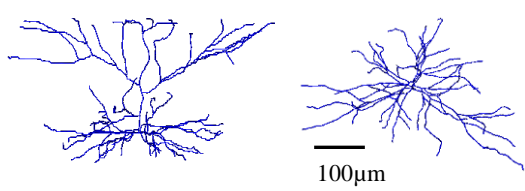
**150710a**



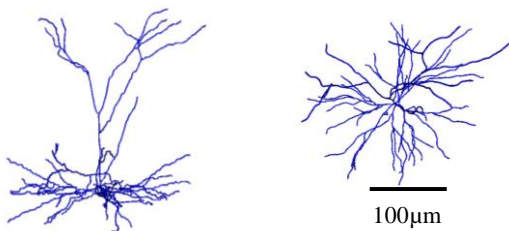
**150720a\_1**



**150720a\_2**



**150720b**



## **אפיון תא עצב פירמידלים בשכבה 3/2 על פי מבנה אנטומי ופלסטיות סינפטית**

רינה ולר

### **תקציר**

רבות נכתב במהלך 150 השנים האחרונות על התאים השכיחים ביותר בקיליפת המוח (Cerebral cortex), תא העצב הפירמידלים. אוכולוסייה נרחבת זו נחשבת כאוכולוסייה בעלת מבנה אחד וייחודי ביותר ביחס לאוכולוסיות תא עצב אחרות כמו התאים המיעכבים (Inhibitory interneurons), אשר למרות חלוקם הקטן יחסית מכלל אוכולוסיית התאים בקיליפת המוח מציגים שונות בגובהה. על אף כל זאת, ישנה שונות בין אוכולוסיות של תאים פירמידלים באזוריים שונים במוח ובשכבות השונות בקיליפת מוח היונק (Neocortex). שונות זו מתבטאת במאפיינים שונים הכוללים את המבנה האנטומי של התא, מיקומו, מקור הקלט, יעד הפלט, פלסטיות ועוד. לכל תא עצב פירמידלי בקיליפת המוח ישנו תפקיד שונה הנגורם ממאפיינים אלו. לכן, תיאור מפורט של המבנה האנטומי והפלסטיות הסינפטית בתאים אלו יוכל להוביל להבנה טובה יותר של רשת תא עצב, פעולתה ותפקידה בקיליפת המוח.

שכבה 3/2 היא אחת משכבות המרכיבות את קליפת מוח היונק ונחשבת כתהנת מפתחה בעיבוד מידע המתקבל מאיזורים נרחבים במוח. אף על פי כן, קיים מידע מוגבל לגבי התאים הפירמידלים המרכיבים שכבה זו. במחקר זה, ביצעו ניתוח רב משתני של המבנה האנטומי וקצב הפלסטיות הסינפטית (Synaptic plasticity) של תא עצב הפירמידלים בשכבה 3/2, המבוסס על הדמיה לארך זמן זמן בחיה השלמה (vivo). כל זאת במטרה לנתח סדרת חוקים המתארים את מבנה התאים ואת השינויים בקשריות עצבית והיחס בין אלו. בנוסף, בדקנו האם חוקים אלו בתאים הפירמידלים מעכבר חלים גם ביונקים אחרים. חוקים אלו מתארים את מבנה הרשת והשינוי בקשריות בשכבה 3/2 חלים באופן מלא אף בתאים דומים בקיליפת המוח של החולדת ושל בני האדם. תיאור זה חיוני להבנת החישוביות, השימושי, התפקיד והקשריות בשכבה מכוננת זו של קליפת מוח היונק.

## **אפיון תאי עצב פירמידים בשכבה 3/2 על פי מבנה אנטומי ופלסטיות סינפטית**

רינה ולר

עבודת גמר מחקרית (תזה) המוגשת כמילוי חלק מהדרישות לקבלת  
התואר "מוסמך האוניברסיטה"

אוניברסיטת חיפה

הפקולטה למדעי הטבע

חוג סגול לננוירוביולוגיה

פברואר, 2019

## **אפיון תאי עצב פירמידלים בשכבה 3/2 על פי מבנה אנטומי ופלסטיות סינפטית**

מאת : רינה ולר

בהנחיית : ד"ר ליאור כהן

עובדת גמר מחקרית (תזה) המוגשת כמלוי חלק מהדרישות לקבלת  
התואר "מוסמך האוניברסיטה"

אוניברסיטת חיפה

הפקולטה למדעי הטבע

חוג סגול לנירוביולוגיה

פברואר, 2019